Charles University

First Faculty of Medicine

Study programme: Biochemistry and Pathobiochemistry

Study branch: YBICH18

UNIVERZITA KARLOVA
1. lékařská fakulta

Ing. Klaudia Kvaková

Fluorescenční nano sondy emitující v blízké infračervené oblasti pro biomedicínské aplikace

Fluorescent nanoprobes emitting in near-infrared region for biomedical applications

Doctoral thesis

Supervisor: Mgr. Petr Cígler, Ph.D.

Prague, 2023

PROHLÁŠENÍ:

Prohlašuji, že jsem závěrečnou práci zpracoval/a samostatně a že jsem řádně uvedla a citovala všechny použité prameny a literaturu. Současně prohlašuji, že práce nebyla využita k získání jiného nebo stejného titulu.

Souhlasím s trvalým uložením elektronické verze mé práce v databázi systému meziuniverzitního projektu Theses.cz za účelem soustavné kontroly podobnosti kvalifikačních prací.

V Praze ……

Klaudia Kvaková

……..

IDENTIFIKAČNÍ ZÁZNAM:

KVAKOVÁ, Klaudia. *Fluorescenční nanosondy emitující v blízké infračervené oblasti pro biomedicínské aplikace. [Fluorescent nanoprobes emitting in near-infrared region for biomedical applications]*. Praha, 2023. 89 stran, 7 příloh. Disertační práce (Ph.D.). Univerzita Karlova v Praze, 1. lékařská fakulta, Ústav organické chemie a biochemie Akademie věd České republiky, v.v.i. Vedoucí práce Cígler, Petr.

ACKNOWLEDGEMENT

First and foremost, I would like to express my deepest gratitude to my supervisor Petr Cígler, whose inspiration, motivation, and support have been invaluable throughout my Ph.D. journey.

Next, I would like to offer my special thanks to Jiří Schimer, whose mentorship and wisdom have enriched my learning experience far beyond what I could have imagined.

I am deeply thankful to the Synthetic Nanochemistry Group for creating a friendly and supportive atmosphere. Specifically, many thanks to Miroslava Štejfová for daily morning coffee sessions, which played a key role in preserving my mental health; Michal Gulka, an exceptional sparring partner, who has endeavored to keep me in shape and enlightened with physics; Marek Kindermann, for his support at conferences around the world and science discussions over beer; and Ema Fialová for her motivational speeches. Many thanks for the support also go to Hana Španielová, Lenka Loukotová, and lastly, Bedřich Formánek.

My gratitude extends to my incredible circle of friends. Marek and Martin deserve a special mention for making memes (not only) about my struggle during the Ph.D. studies and entertaining the rest of our friends. I am grateful to Soňa for reminding me that I chose to study Ph.D.; therefore, I should not complain about it. I also thank Muša for her unique motivational style - telling me that staying in Valaská would be worse than studying Ph.D. I would also thank Helena for her emotional support and Monika for her valuable (spiritual) advice.

Special acknowledgment to my beloved Laetitia (kočička) for her everlasting patience, motivation & encouragement. Furthermore, for creating a pleasant environment and pushing me to be more active, especially while writing this thesis. Merci Bochu!

Lastly, I would like to thank my family for their support during my studies.

This accomplishment would not have been possible without you all! Thank you again!

ABSTRACT

The primary focus of this thesis is to conduct an in-depth investigation into the capabilities of near-infrared photoluminescent (PL) nanoprobes and their application in biomedicine. Specifically, this research explores the potential of fluorescent nanodiamonds (FNDs) and gold nanoclusters (AuNCs). First, the thesis examined the potential of FNDs for *in vivo* visualization of mice sentinel lymph nodes (SLNs). The study observed that FNDs modified with mannose exhibited greater uptake by macrophages and improved retention within SLNs compared to non-mannosylated FNDs. In addition, FNDs possess a remarkable capacity to accurately measure cellular temperature as was demonstrated by local temperature variation measurements associated to hippocampal neurons firing. Furthermore, the study explored the potential of AuNCs as viable tools for cellular imaging. A simple synthetic approach was developed to create AuNCs with enhanced stability, ligand-based PL enhancement, and prolonged fluorescence lifetime. The thesis also describes the reversible photo- and thermal-induced effects on the PL properties of the synthesized AuNCs. Additionally, the enhancement of AuNCs' PL through their combination with plasmonic nanostructures, specifically gold nanorods, was described. Lastly, a successful visualization of the intracellular internalization of the AuNCs was achieved. This thesis presents valuable insights about FNDs and AuNCs as sophisticated PL nanoprobes for biomedical applications and is relevant mainly for bioimaging, diagnostics, nano-thermometry, and the general design of a functional nano-bio interface.

Key words: fluorescent nanodiamonds, photoluminescent gold nanoclusters, surface modifications, sentinel lymph nodes, nano-thermometry, fluorescent imaging

ABSTRAKT

Hlavním cílem této práce je podrobný výzkum fluorescenčních nanosond emitujících v blízké infračervené oblasti a jejich využití v biomedicíně. Jsou studovány zejména fluorescenční nanodiamanty (FND) a zlaté nanoklastry (AuNC). Nejprve byl zkoumán potenciál FND pro *in vivo* vizualizaci sentinelových lymfatických uzlin v myším modelu. Tato studie ukázala, že FND modifikované manózou vykazují vyšší internalizaci makrofágy a lepší retenci v sentinelových lymfatických uzlinách v porovnání s výchozími FND. Kromě využití v bio-zobrazování byly FND použity i pro přesné měření teploty v buňkách s difrakčním rozlišením. V této práci byly FND použity jako sondy pro lokální měření změn teploty v důsledku aktivity hipokampálních neuronů. Dále byl zkoumán potenciál AuNC, jakožto možných fluorescenčních značek pro značení a zobrazování buněk. Jednoduchou syntetickou cestou byly připraveny stabilní AuNC. Dalšími modifikacemi pomocí různých ligandů bylo dosaženo zvýšení intenzity fotoluminiscence a prodloužení doby života fotoluminiscence. Práce dále popisuje reverzibilní světelně a tepelně indukované účinky na fotoluminiscenční vlastnosti syntetizovaných AuNC. Bylo též prokázáno zesílení fotoluminiscence AuNC pomocí použití konjugace s plazmonickým systémem – zlatými nanotyčemi. Nakonec byla dosažena internalizace připravených AuNC do buněk a jejich následná vizualizace. Tato práce přispívá k probíhajícímu vývoji FND a AuNC jakožto fluorescenčních nanosond pro biomedicínské aplikace, a má relevanci především pro zobrazování v biologických systémech, diagnostiku, nanotermometrii, a obecně pro design funkčního nano-bio rozhraní.

Klíčová slova: fluorescenční nanodiamanty, fotoluminiscenční zlaté nanoklastry, povrchové modifikace, sentinelové lymfatické uzliny, nanotermometrie, fluorescenční zobrazování

LIST OF ABBREVIATIONS

5-ALA	5-aminolevulinic acid
ATRP	atom transfer radical polymerization
AuNC	gold nanocluster
AuNP	gold nanoparticle
AuNR	gold nanorod
AuNR@AuNCs	complex of gold nanorod
Au@SiO_2NR	silica-coated gold nanorod and gold nanoclusters
BSA	bovine serum albumin
CLSM	confocal laser scanning microscope
CT	computed tomography
CTRL	control
CVD	chemical vapor deposition
DLS	dynamic light scattering
DNDs	detonation nanodiamonds
EDC	1-ethyl-3-(dimethylaminopropyl) carbodiimide hydrochloride
EQY	external quantum yield
ESI-MS	electrospray ionization - mass spectrometry
FDA	food and drug administration
FGS	fluorescence-guided surgery
FND-p	polymer-coated fluorescent nanodiamonds
FND-p-Man	mannosylated polymer-coated fluorescent nanodiamonds
FNDs	fluorescent nanodiamonds
FRET	Förster resonance energy transfer
GSH	glutathione
HAE	heavy atom effect
HOMO	highest occupied molecular orbital
HPHT	high-pressure high-temperature
HR-STEM	high-resolution scanning transmission electron microscopy
ICG	indocyanine green
ICP-OES	inductively coupled plasma-optical emission spectroscopy
ISC	intersystem crossing
LN	lymph node
LUMO	lowest unoccupied molecular orbital
MRI	magnetic resonance imaging
MW	microwave
ND	nanodiamond
NIR	near-infrared
NMR	nuclear magnetic resonance
NP	nanoparticle
NV	nitrogen-vacancy
NVN	nitrogen-vacancy-nitrogen
ODMR	optically detected magnetic resonance

PA	polyarginine
PAH	poly(allylamine hydrochloride)
PDA	polydopamine
PEG	polyethylene glycol
PEI	polyethyleneimine
PG	polyglycerol
PHPMA	poly[N-(2-hydroxypropyl) methacrylamide]
PL	photoluminescent
PLE	photoluminescence excitation
PLGA	poly(lactic-co-glycolic acid)
PLL	poly-L-lysine
PL-LSPR	photoluminescence – localized surface plasmon resonance
PNIPAM	poly(N-isopropyl acrylamide)
QD	quantum dot
RAFT	reversible addition-fragmentation chain transfer
SiNP	silica nanoparticle
SiV	silicon-vacancy
SLNB	sentinel lymph node biopsy
SLN	sentinel lymph node
SPR	surface plasmon resonance
TPP	3-(aminopropyl) triphenylphosphonium
TTX	tetrodotoxin

TABLE OF CONTENTS

1 INTRODUCTION.....15

1.1 Fluorescent dyes and fluorescent probes.....15

1.2 Fluorescence imaging *in vitro* 16

1.3 Fluorescence imaging *in vivo* 18

1.4 NIR emitting probes for biomedical applications 20

1.4.1 Molecular probes.....21

1.4.2 Nanoparticles.....22

1.5 Fluorescent nanodiamonds 25

1.5.1 Structure and properties of FNDs.....25

1.5.2 Production and surface modifications of NDs 26

1.5.3 Optical properties of NV centers.....27

1.5.4 Polymer coating & biomedical applications of FNDs 29

1.6 Gold nanoclusters 32

1.6.1 Biocompatibility of AuNCs 32

1.6.2 Size and optical properties of AuNCs.....33

1.6.3 Modifications of AuNCs.....34

1.6.4 Biomedical applications of AuNCs.....36

1.7 Visualization of sentinel lymph nodes 37

1.7.1 Histology of sentinel lymph nodes.....37

1.7.2 Detection of sentinel lymph nodes.....38

1.7.3 Fluorescence-guided surgery.....40

2 AIMS OF THE THESIS.....42

3 METHODS 43

4 SUMMARY OF THE RESULTS AND DISCUSSION.....44

4.1 Visualization of Sentinel Lymph Nodes with Mannosylated Fluorescent Nanodiamonds 46

4.2 Nanodiamond–Quantum Sensors Reveal Temperature Variation Associated to Hippocampal Neurons Firing 51

4.3 Synthesis of Near-Infrared Emitting Gold Nanoclusters for Biological Applications. 53

4.4 Inverse Heavy-Atom Effect in Near Infrared Photoluminescent Gold Nanoclusters. 56

4.5 Reversible Photo- and Thermal-Effects on the Luminescence of Gold Nanoclusters: Implications for Nanothermometry. 59
4.6 Optically Coupled Gold Nanostructures: Plasmon Enhanced Luminescence from Gold Nanorodnanocluster Hybrids.....62
4.7 Towards Site-specific Emission Enhancement of Gold Nanoclusters Using Plasmonic Systems: Advantages and Limitations.....65
5 CONCLUSIONS..... 67
6 LIST OF PUBLICATIONS..... 69
7 REFERENCES..... 70
8 LIST OF APPENDICES..... 88

1 INTRODUCTION

1.1 Fluorescent dyes and fluorescent probes

Fluorophores are indispensable tools in biological sciences, particularly in microscopy, cell biology, and molecular biology research. These species can absorb light at specific wavelengths and emit light at higher wavelengths almost instantaneously, providing means to visualize and track various biological processes. Fluorophores include a broad range of chemically diverse compounds, including small organic molecules (e.g., fluorescein, rhodamine, cyanine), amino acids (tryptophan, tyrosine, phenylalanine), biological fluorophores - fluorescent proteins (e.g., green fluorescent protein, red fluorescent protein), or inorganic compounds such as quantum dots. Fluorescent nanoparticles (NPs) have become attractive for these applications because of their improved optical properties and non-toxicity. Various factors can be used to distinguish between fluorophores and fluorescent nanoprobes, as they exhibit significant differences. Understanding the properties, such as excitation, emission wavelength, quantum yield, extinction coefficient, photostability, and fluorescence lifetime, are essential for their effective use in biological or any other applications (Lakowicz, 2009; Valeur and Berberan-Santos, 2012).

Absorption and emission spectra are governed by the electronic structure of a molecule and energy differences between its electronic states, and they define the properties of fluorophores. The absorption spectrum represents the range of wavelengths fluorophore can absorb, and the emission spectrum shows wavelengths at which the emitted light can occur. There is one main difference between absorption and emission; the fluorophore's surroundings affect the emission due to potential energy transfer interactions. When a fluorophore absorbs light, it transits from its ground state to an excited state. After reaching the excited state, the fluorophore typically returns to its ground state by emitting a photon, thus producing fluorescence. During this relaxation process, energy losses occur, therefore, the emitted light has lower energy, and hence a longer wavelength, than the absorbed light. The emission maximum is always a longer wavelength than the absorption maximum – this red-shift phenomenon is known as the Stokes shift (Lakowicz, 2009).

Quantum yield is defined as the number of photons emitted (i.e., in the form of fluorescence) divided by the number of photons absorbed, and it describes the efficiency of fluorophores converting absorbed light into fluorescence (Villamena, 2017). Values of the quantum yield range between 0 and 1, where 1 means 100% efficiency. The probability of photon absorption is not the same for all the fluorophores and is described by a measurable characteristic called extinction coefficient (ε). The extinction coefficient value gives information about the photon absorption capacity of the fluorophore at a particular wavelength (Lakowicz, 2009). If quantum yield is related to the extinction coefficient, another significant characteristic for fluorescent probes called brightness is obtained. The brightness can provide us with higher sensitivity for fluorescent detection (Waters and Wittmann, 2014). Highly bright fluorescent probes provide an additional advantage for imaging in biological systems (Lakowicz, 2009).

Another crucial parameter describing the electron transition process is fluorescence lifetime. It is an intrinsic property of fluorophores, defined as the characteristic time that a molecule remains in its excited state before returning to the ground state (Becker, 2012; Datta et al., 2020). Fluorescence lifetime is given by the structure of the fluorophore, and it is not dependent on the fluorophore concentration and fluorescence intensity, which is a great advantage. Moreover, excitation wavelength, excitation type (single or multi-photon), light exposure time, and photobleaching typically do not affect fluorescence lifetime. However, fluorescence lifetime can be influenced by the microenvironment around a fluorophore (e.g., by temperature or by the presence of quenchers) (Berezin and Achilefu, 2010).

The general properties of fluorophores mentioned above are crucial for their selection for different applications. For successful fluorescence imaging, fluorescent probes must fulfill more requirements besides high brightness and quantum yield, such as good photostability, bio-stability, water solubility, biocompatibility, and specificity (Zhang et al., 2022).

1.2 Fluorescence imaging *in vitro*

Fluorescent imaging *in vitro* provides a versatile tool for studying cellular structures and processes in a highly controlled environment, facilitating precise manipulation and observation. While the technique offers high-resolution imaging

and the ability to manipulate experimental conditions, it also faces several challenges that can impact the quality and interpretability of results.

High illumination intensities during fluorescence imaging can cause fluorophore blinking, originating in triplet state intersystem crossing (ISC). ISC is a quantum mechanical process where the electron transitions from the excited singlet state (S1) to an excited triplet state (T1), this transition involves a spin flip. While the electron is in the triplet state, a fluorophore is effectively "off". Electron can return to the ground state (S0) *via* phosphorescence, which is much slower than fluorescence, or *via* a non-radiative process (Figure 1). After that, a fluorophore can again absorb a photon and emit fluorescence, returning to the "on" state. In some cases, fluorescence fading can be observed, resulting in irreversible loss of fluorescence called photobleaching. Photobleaching is an intrinsic event induced by light and causes destruction that occurs in the excited state of a fluorophore. It can significantly hinder the ability to track processes over time, especially for long-term live-cell imaging. Photobleaching is a common issue in fluorescence imaging and can be minimized by optimization of acquisition; nevertheless, photo blinking (switching) and photobleaching limit the experimental performance of fluorophores (Zheng and Lavis, 2017).

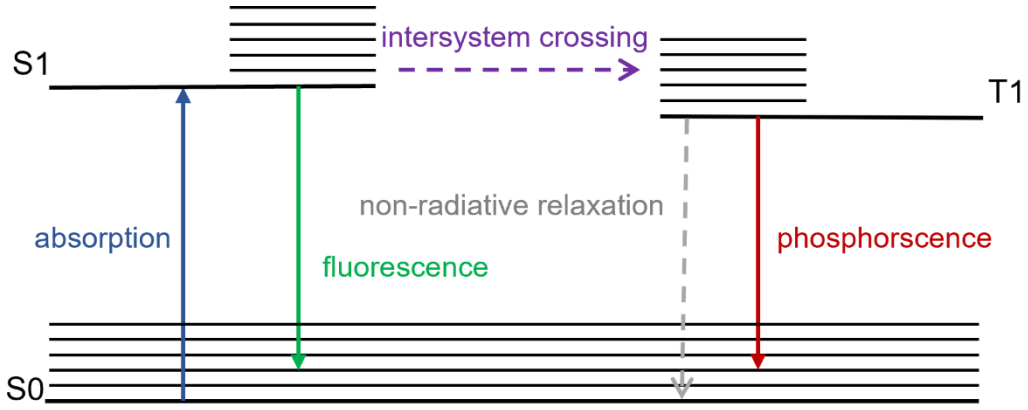

Figure 1: Simplified Jablonski diagram illustrating radiative (solid line) and non-radiative (dashed line) processes that may occur after photon absorption. Reproduced and adapted from the literature (Lakowicz, 2009)

Another frequently observed phenomenon that causes a decrease in fluorescence intensity is called fluorescence quenching. Plenty of mechanisms can decrease fluorescence intensity, such as collisional (dynamic) quenching, static quenching, and Förster resonance energy transfer (FRET). Collisional quenching is observed when the fluorophore is in contact with some molecule in a solution that

deactivates it after their contact. Usually, the quencher diffuses to the fluorophore during the excited state period, leading to non-radiative energy dissipation. Static quenching occurs when a fluorophore and quencher form a non-fluorescent complex. FRET involves energy transfer from an excited donor fluorophore to a nearby acceptor molecule, which can result in quenching if the acceptor does not fluoresce. This principle is often utilized in biological research to study protein-protein interactions, but unwanted FRET can interfere with imaging. Another type of fluorescence quenching is self-quenching which occurs due to energy loss through collisions between the excited and ground state molecules of fluorophores. Quenching can be influenced by environmental factors such as temperature, pH, and the presence of specific ions or molecules. *In vivo* imaging then bring an additional layer of complexity (Lakowicz, 2009; Zhang et al., 2022).

Natural emission of light by biological structures after light absorption, autofluorescence, is another challenge. This background noise can interfere with the fluorophore signal, which usually decreases the signal-to-noise ratio and makes detecting the target more difficult. Specific biological sample preparation and image processing techniques can minimize autofluorescence (Monici, 2005).

Excitation light can also cause phototoxicity - damage induced in biological specimens, especially in live-cell imaging. Light absorption can lead to the production of reactive oxygen species, causing cellular damage and creating measurement artifacts. Minimizing phototoxicity requires careful optimization of imaging parameters, but it can limit the duration of imaging sessions and the types of fluorophores that can be used (Laissue et al., 2017; Magidson and Khodjakov, 2013).

Advances in fluorescent probe design, imaging technologies, and sample preparation methods continue to improve our ability to overcome these challenges, expand the possibilities of *in vitro* experiments and enable us to improve *in vivo* imaging.

1.3 Fluorescence imaging *in vivo*

In vivo imaging provides a unique opportunity to study biological processes in their natural context. For example, we can observe tissue development, disease progression, biodistribution and treatment responses, which is impossible during *in vitro* fluorescence imaging. However, with system complexity, more challenges

occur (Kim and Kim 2021). The most significant factors influencing fluorescence signal during *in vivo* fluorescence imaging are light absorption, light scattering, and reabsorption of emitted photons (Lakowicz, 2009).

The biological environment itself poses significant challenges for *in vivo* fluorescence imaging. The delivery of fluorophores to the target of interest can be complicated by biological barriers such as the blood-brain barrier or the cell membrane and the organism's immune response (Ntziachristos, 2010). Furthermore, the complex and dynamic nature of the i*n vivo* environment, including factors such as pH, ion concentration, and protein binding, strongly impacts the fluorophore's fluorescence properties (Lakowicz, 2009).

Biological tissues, specifically their chromophores such as hemoglobin, melanin, and water, absorb light at specific wavelengths. Such absorption reduces the amount of light available for fluorophore excitation during imaging and decreases the detected fluorescence signal. Moreover, tissue absorption causes autofluorescence which is challenging for *in vivo* experiments due to additional sources of autofluorescence, such as blood and connective tissues and a wider variety of autofluorescent molecules (Jacques, 2013). Furthermore, excessive light absorption can cause tissue damage or injury in animal models (Feng et al., 2021).

Light scattering occurs when light encounters the tissue, especially its inhomogeneities. This phenomenon leads to a deviation from its initial propagation direction. Light scattering is particularly significant in biological tissues due to cellular structures of various sizes and refractive indexes (Tuchin, 2007). Scattering decreases the intensity of incident light reaching the target, reducing the excitation of fluorophores and, thus, the detected fluorescence signal. Furthermore, scattering distorts the spatial distribution of both the excitation and emitted light, leading to a loss of resolution and difficulties in determining the exact origin of the fluorescence signal, a problem known as the inverse problem (Jacques, 2013; Ntziachristos, 2010). Both absorption and scattering are wavelength-dependent, with shorter wavelengths generally experiencing higher levels of scattering and absorption. This is particularly problematic in the visible range, where most conventional fluorophores absorb. The penetration of visible light is only a few hundred micrometers. Thus, deeper tissue imaging often requires near-infrared (NIR) emitting fluorophores operating in a wavelength range where scattering and absorption are minimized (Refaat et al., 2022).

In complex biological systems, emitted photons of excited fluorophores can be absorbed by another fluorophore, and the photons will not reach the detector, but it leads to the excitation of the second fluorophore. Such an event is called the reabsorption of emitted photons and complicates fluorescence imaging. The reabsorption process depends on the concentration and distribution of fluorophores and the overlap between one fluorophore's emission spectrum and another's absorption spectrum. The reabsorption of emitted photons can lead to changes in the observed fluorescence intensity and lifetime and can shift the observed emission wavelength. This shift can be used to distinguish between directly excited fluorescence and fluorescence resulting from reabsorption. The reabsorption phenomenon increases with the path length of the emitted photon through the tissue. This effect, combined with the tissue's scattering and absorption of light, can lead to a significant loss of signal (Lakowicz, 2009).

In summary, fluorescence-based imaging has gained increasing attention among visualization methods in the last decades because it is a versatile, real-time, and non-invasive technique that enables the localization of biological processes and their subsequent visualization with high sensitivity. High-performance NIR-emitting fluorescent probes are among the most promising future agents. Therefore, they are intensively studied for their advantages, such as deeper tissue penetration and higher-resolution imaging (Yue et al., 2018).

1.4 NIR emitting probes for biomedical applications

Advances in NIR fluorescence imaging have mainly focused on compounds emitting in the so-called first NIR window (650-900 nm). The range of NIR fluorescent probes is extensive and constantly expanding, reflecting the evolving needs in biomedical imaging. NIR fluorescent probes can be divided into molecular probes (organic dyes) and NP-based fluorescent probes. Unique properties characterize each group of probes and determine their applications (Zheng et al., 2022). This section will discuss the differences between molecular dyes and NP-based fluorescent probes, primarily focusing on their size, selectivity, and toxicity.

1.4.1 Molecular probes

Molecular probes, being small molecules, offer numerous advantages for bioimaging applications. Their compact size facilitates improved tissue penetration, cellular uptake, and access to intracellular targets. Additionally, their small size contributes to faster blood circulation and efficient renal clearance, minimizing the potential for accumulation in the body. However, rapid clearance can limit their use in long-term imaging applications. The small size of molecular probes also limits their modification potential, consequently reducing their targeting possibilities. Functionalization of the dye can cause a significant size increase and drastically alter molecular dye properties (Yang et al., 2022).

Precise imaging of specific targets in biological systems demands molecular probes with high selectivity. Molecular probes can be customized to exhibit high specificity for specific targets by conjugating targeting ligands such as antibodies (Cilliers et al., 2017) or peptides (Berezin et al., 2011) with a dye structure. However, as mentioned above, molecular dyes' modification possibilities are limited. In addition, the selectivity of molecular probes is often decreased mainly due to non-specific interactions with biological molecules and rapid clearance from the body (Yang et al., 2022).

Toxicity plays a critical role in determining the safety and applicability of visualization tools in bioimaging. The level of toxicity exhibited by these tools directly impacts their usability and potential impact on biological systems. The potential toxicity of molecular probes depends on their specific molecular structures. Organic dyes can be designed to minimize toxicity, but some may still pose toxicity risks due to the potentially harmful metabolites. The risk of phototoxicity, where light exposure leads to toxic reactions, must also be taken into consideration in the design and use of NIR-emitting molecular probes (Alford et al., 2009; Broadwater et al., 2019).

In the field of bioimaging and biomedicine, molecular fluorescent probes that emit in the NIR region have garnered significant attention. These probes primarily consist of cyanine dyes (Gopika et al., 2021), squaraine dyes (Yadav et al., 2020), porphyrin derivatives, and phthalocyanines. Their unique properties and NIR emission make them particularly suitable for various applications in biological imaging and medical research. Cyanine dyes are the NIR region's most frequently used molecular fluorescent probes. They exhibit high molar absorption coefficients,

strong fluorescence, and good photostability (Gopika et al., 2021). Cyanine dyes include indocyanine green (ICG), an FDA-approved dye that has been used extensively in medical diagnostics, for example, in fluorescence-guided abdominal surgery (Van Manen et al., 2018) and intraoperative tumor detection (Nagaya et al., 2017).

Squaraine dyes exhibit high photostability, strong NIR fluorescence, and large Stokes shifts, which minimize self-quenching and autofluorescence. They can be functionalized, allowing for the attachment of various targeting ligands. Their potential has been demonstrated in various bioimaging applications (Yadav et al., 2020).

Despite massive progress in this field, challenges persist. The higher degree of control over molecular design could allow the development of highly selective NIR emitting molecular probes, distinguishing specific cell types, physiological states, or molecular pathways, and help to enhance dyes' photostability and brightness while reducing their toxicity.

1.4.2 Nanoparticles

The size of NIR-emitting NPs plays a crucial role in determining their imaging capability and biodistribution, and it exhibits significant variation within the NP group. Larger nanoparticle sizes offer advantages such as providing a platform for surface modifications, influencing renal clearance, and extending circulation time compared to small molecular dyes. These attributes make larger NPs well-suited for certain applications in bioimaging and biomedicine. However, their larger size may limit tissue penetration and lead to non-specific accumulation in organs, particularly the liver and spleen, raising concerns over toxicity (Haute and Berlin, 2017).

NPs can be functionalized with various targeting ligands, including antibodies, peptides, and small molecules, that can specifically bind to biomarkers in the target tissue, resulting in their high specificity. However, high specificity is a complex problem that depends not only on surface chemistry but also on the size and shape of NPs (Albanese and Chan, 2011). The complexity of NP synthesis and potential heterogeneity may challenge their reproducibility and scalability, which can be very problematic (Farokhzad and Langer, 2009).

The toxicity of NPs primarily depends on their composition, surface properties, size, and shape. Certain NP materials, such as cadmium-based quantum dots, have been associated with significant toxicity, primarily due to the release of toxic ions (Liu and Tang, 2020). Consequently, research has shifted towards developing biocompatible NIR-emitting NPs, such as organic dyes encapsulated in biocompatible polymers (Reisch and Klymchenko, 2016) or silica (Khatoon et al., 2018), ultrasmall gold nanoclusters (Van De Looij et al., 2022) or fluorescent nanodiamonds (Mitura and Włodarczyk, 2018). While NPs offer lower toxicity profiles compared to some other imaging agents, the long-term safety of NPs still requires extensive investigation. The surface properties of NPs also significantly impact their toxicity. NPs with hydrophilic surfaces are generally more biocompatible than hydrophobic ones. Hydrophobic NPs tend to aggregate in biological systems, which can lead to blockages in small blood vessels (Caracciolo, 2018).

Quantum dots (QDs) are semiconductor NPs, typically ranging in size from 2 to 10 nm, exhibiting size-dependent optical and electronic properties. The ability to fine-tune these properties, particularly the emission spectrum, by altering the size and composition of the QDs, makes them versatile candidates for a broad range of applications, including bioimaging. QDs enable multiplexed imaging – the simultaneous observation of multiple targets in a single experiment. QDs are far more photostable than conventional organic dyes and fluorescent proteins. Despite their many advantages, their potential toxicity is a significant challenge in using QDs for bioimaging. Many QDs are composed of heavy metals such as cadmium and selenium, which can pose health risks if not appropriately encapsulated or surface-modified. QDs also often require surface modification to increase their stability and biocompatibility in biological environments. However, these modifications can alter the photophysical properties of QDs, potentially limiting their effectiveness as imaging agents (Namdari et al., 2017; Pohanka, 2017; Wagner et al., 2019). QDs have been extensively studied in tumor imaging (McHugh et al., 2018), cell tracking (Bruns et al. 2017), and immunoassays (Zhang et al. 2016).

Polymer NPs are materials from the polymer matrix, providing structural stability and can, for example, encapsulate NIR fluorescent dyes. The common polymers used in the synthesis of these NPs include biocompatible and biodegradable poly(lactic-co-glycolic acid) (PLGA), polyethylene glycol (PEG) (FDA-approved

polymer), and styrene. The encapsulation of NIR dyes within NPs serves several purposes: it protects the dye from degradation, enhances its photostability, and helps to prevent direct interaction of the dye with biological tissues (Reisch and Klymchenko, 2016). Besides NIR fluorescent dyes, QDs were also encapsulated by polymers to protect them and increase their biological stability (Tomczak et al., 2013; Yang et al., 2019). The surface of polymer NPs can be functionalized with various ligands or antibodies for targeted imaging and drug delivery. Furthermore, they can be designed to respond to specific physiological environments or to target specific cells or tissues. However, synthesizing polymer NPs with consistent properties (size, shape, fluorescence characteristics) can be challenging, influencing the reproducibility of bioimaging results. Encapsulating NIR dyes into NPs without causing quenching of the fluorescence or preventing leaking of the dye remains a technical challenge. If the encapsulated dye leaks out of the nanoparticle, it may interact with cells and tissues, potentially leading to cytotoxic effects. Therefore, the potential toxicity will strongly depend on each NPs formulation and must be evaluated before the application in biological systems (Reisch and Klymchenko, 2016).

Similarly, like in the case of polymer NPs, silica nanoparticles (SiNPs) can provide a stable platform for the incorporation of organic dyes to protect them from photobleaching, enzymatic degradation, and interaction with biological molecules, thus maintaining their fluorescence and stability over time. The silica matrix enables controlled dye-doping, limiting dye-dye interactions that can result in self-quenching. Consequently, SiNPs can exhibit enhanced brightness and tunable fluorescence emission, which is vital for high-resolution imaging (Gubala et al., 2020). SiNPs can also be toxic, depending on their charge, size, porosity, and surface modifications. Polymer coating strategies are often employed to increase SiNPs biocompatibility and reduce cytotoxicity in biological systems (Nadal et al., 2022). SiNPs offer tunable size and porosity so that they can show non-toxicity. However, achieving precise size control resulting in uniform size distribution during synthesis can be challenging (Khatoon et al., 2018). Moreover, the polymer coating can (negatively) impact incorporated dye, affecting SiNPs' use in bioimaging applications (Kohle et al., 2019).

Fluorescent nanodiamonds (FNDs) possess several properties that set them apart from other near-infrared emitting nanoprobes, such as unlimited photostability (Reineck et al., 2016), near-quantitative quantum yield (Yu et al., 2005), intrinsic biocompatibility (Barone et al., 2018) and hemocompatibility (Li et al., 2013). FNDs do not show liver toxicity or cause systemic inflammation (Zhu, 2012). Their size varies from a few nanometers to several hundred nanometres, and their optimal size depends on the specific requirements of the bioimaging applications. One of the essential properties that depends on the size of FNDs is their brightness (Reineck et al., 2019).

Ultrasmall photoluminescent AuNCs have also been widely studied for their unique properties, making them advantageous compared to other NIR-emitting nanoprobes and molecular dyes. Unlike molecular probes, AuNCs have a huge modification potential which is crucial for targeting (Pang et al., 2022) or tuning emission properties (Yuan et al., 2020) even though they have molecular size (Van De Looij et al., 2022). Their long emission lifetime enables time-resolved imaging techniques and can eliminate short-lived autofluorescence (Zhou et al., 2019). Similarly, like FNDs, they are photostable (Yuan et al., 2020), biologically stable, and inherently biocompatible (Zhang et al., 2014).

1.5 Fluorescent nanodiamonds

1.5.1 Structure and properties of FNDs

The appeal of FNDs stems from their distinctive optical properties and their favorable behavior when interacting with biological systems. A fundamental understanding of the crystalline structure is required to realize their full potential in the applications.

Nanodiamonds (NDs) are nano-sized diamond particles, and at the atomic level, they share the same cubic crystal structure as bulk diamonds. Each carbon atom is tetrahedrally coordinated in this configuration, which means that it is bonded to four other carbon atoms (sp^3 carbon hybridization). Each carbon atom contributes one electron to each of the four covalent bonds, leading to a highly stable structure. The diamond structure's high symmetry and strong covalent bonding confer exceptional hardness and high thermal conductivity, which are retained even at the nanoscale level.

The diamond lattice stability is one of the reasons behind the chemical inertness of diamonds and their nanoscale counterparts. The tightly packed carbon atoms limit the available reaction sites and prevent the interaction of FNDs with other chemical species (Shenderova and McGuire, 2015). Chemical inertness is essential for FNDs' biocompatibility and non-toxicity. It was shown that FNDs can be internalized by cells without disrupting normal cellular functions. FNDs do not elicit a strong immune response (Chipaux et al., 2018). Furthermore, the surface of FNDs can be modified, and functionalized with various biomolecules, enhancing their biocompatibility even further and providing specific interaction with cellular targets for more advanced bio-applications (Neburkova et al., 2017).

1.5.2 Production and surface modifications of NDs

While the crystalline structure of NDs is important, the unique properties that make these NPs attractive in applications are their impurities and defects. The impurities and defects depend on the ND production method and the subsequent treatment. NDs can be produced by various methods, each with a different impact on the ND properties. The most common types of NDs are high-pressure high-temperature (HPHT) NDs, detonation nanodiamonds (DNDs), and chemical vapor deposition (CVD) NDs. HPHT NDs result from micron-sized diamond ball milling prepared by the HPHT method. During the HPHT process, usually, graphite is converted to diamond under pressure approx. several GPa and temperature approx. 1500 °C. DNDs are synthesized from a carbon of explosives, most commonly hexogen with trinitrotoluene. This method, called detonation, involves the incomplete combustion of the explosives in a closed container, resulting in the formation of ND crystals. Both HPHT NDs and DNDs are commercially available. HPHT NDs are generally larger than DNDs and show high purity and crystallinity. Moreover, they contain a high amount of nitrogen impurities, resulting in a possible nitrogen-vacancy (NV) center creation. (Nunn et al., 2017). The generation of CVD NDs commences with the fabrication of a polycrystalline chemical vapor deposition film, followed by its disintegration to yield NDs. The CVD process allows for precise control over the material's properties, such as purity, crystallinity, and doping, by manipulating the process parameters. This method is often used to produce NDs with silicon-vacancy (SiV) centers which show superior fluorescence properties. However, the CVD process is relatively high-price, and the deposition rate is slow (Qin et al., 2021).

In addition to nitrogen or silicon impurities in the crystalline lattice, FNDs may also contain surface impurities, including sp^2 hybridized carbon atoms (graphite). These surface impurities generally make up a relatively small proportion compared to sp^3 carbon atoms. However, several approaches were developed to reduce or remove sp^2 carbon impurities from the surface of FNDs. One of the most common direct surface modifications is oxidation which is done by treating FNDs with strong oxidants such as acids. This process removes non-diamond carbon and enriches the surface with oxygen-containing functional groups such as carboxyls (-COOH) and carbonyls (C=O). Introduced carboxylic groups can be used for further covalent modifications with other molecules. Another frequently used treatment is hydrogenation. Hydrogen atoms bond to available carbon sites on the FND surface during hydrogenation. The process usually requires a catalyst and must be carried out under specific temperature and pressure conditions. Other FND surface treatment modifications were described, including fluorination, amination, and silanization (Krueger, 2017).

1.5.3 Optical properties of NV centers

The main emphasis of this doctoral thesis will be on HPHT NDs due to their significant presence of NV centers. The NV centers are the origins of fluorescence and quantum sensing properties making FNDs attractive in bioimaging and quantum sensing applications (Turner, 2017). NV centers in NDs are created in a two-step process. First, carbon atoms are substituted with nitrogen atoms, which is usually accomplished during the NDs production. Subsequently, vacancies formation and migration are necessary. Irradiation of NDs with high-energy particles instigates the displacement of carbon atoms from the lattice, consequently leading to the generation of vacancies. Following thermal annealing process results in the migration of vacancies through the lattice, some vacancies will position themselves adjacent to nitrogen atoms, thereby forming NV centers (Treussart and Vlasov, 2017).

As described previously, NV centers can exist in two charge states: neutral (NV^0) and negatively charged (NV^-). The electronic structure of these two states is different and determines their potential use in quantum sensing. The neutral NV^0 center consists of five electrons, two unbounded valence electrons from nitrogen (creating a lone pair), and three electrons from the carbon atoms surrounding the vacancy (resulting in an unpaired electron). The NV^0 center thus has a spin 1/2

ground state, however no detectable electron paramagnetic resonance. The NV^- center has an additional donor electron forming a ground state triplet (S = 1), implying three possible spin states ($|m_s = 0\rangle$, $|m_s = +1\rangle$, and $|m_s = -1\rangle$).

The NV^- electron can be optically excited from its ground state to the excited state. Its de-excitation results in the emission of a red photon (zero phonon line of 637 nm with broad sideband). These transitions are spin-preserving, meaning the spin does not change its state. This process provides stable emission, unaffected by photobleaching or blinking, which is important for applications of FNDs as fluorescent probes. However, there is an additional decay path through a metastable singlet state without the emission of a visible photon. This "dark" transition is preferential for the $|m_s = \pm1\rangle$ sublevels, yet the electrons decay predominantly to the $|m_s = 0\rangle$ spin state (Figure 2A). This characteristic enables optical readout of the NV^- center's spin, as the $|m_s = \pm1\rangle$ sublevels are darker than the $|m_s = 0\rangle$ state, and also spin initialization, as the spin is polarized to the $|m_s = 0\rangle$ state after few optical cycles. Remarkably, the NV^- center thus fulfills the two main prerequisites of a qubit and works at room temperature (Segawa and Igarashi, 2023).

Moreover, the occupation of the $|m_s = 0\rangle$ and $|m_s = \pm1\rangle$ sublevels can be altered with a resonant microwave (MW) field enabling optically detected magnetic resonance (ODMR). This method involves exciting (polarizing) the NV^- center with a green (typically 532 nm) pump laser while sweeping the MW frequency. When the MW frequency matches the energy between the $|m_s = 0\rangle$ and $|m_s = \pm1\rangle$ transition of the ground state (D_{gs}), the occupation of the $|m_s = \pm1\rangle$ sublevel increases resulting in lower photon collection – i.e., dip in the ODMR spectrum at the resonant frequency (Figure 2B). In the absence of a magnetic field, the $|m_s = \pm1\rangle$ sublevels have the same energy. However, in a magnetic field, the $|m_s = \pm1\rangle$ degeneracy is lifted, resulting in a distinct energy separation between the $|m_s = +1\rangle$ and $|m_s = -1\rangle$ spin states (Zeeman splitting). Subsequently, two dips are observable in the ODMR spectrum ($|m_s = 0\rangle \rightarrow |m_s = +1\rangle$ and $|m_s = 0\rangle \rightarrow |m_s = -1\rangle$ transitions), which provides means of sensitive magnetic field detection as their splitting is linearly proportional to the projection of the B-field to the NV^- axis. Additionally, the value of D_{gs} is temperature-dependent, enabling temperature sensing by observing the shift of the ODMR resonant frequencies. Consequently, FNDs are promising for quantum sensing applications for both magnetic noise detection, e.g., pulsed-ODMR methods (Barton et al., 2020), and for local temperature measurements (Petrini et al., 2022).

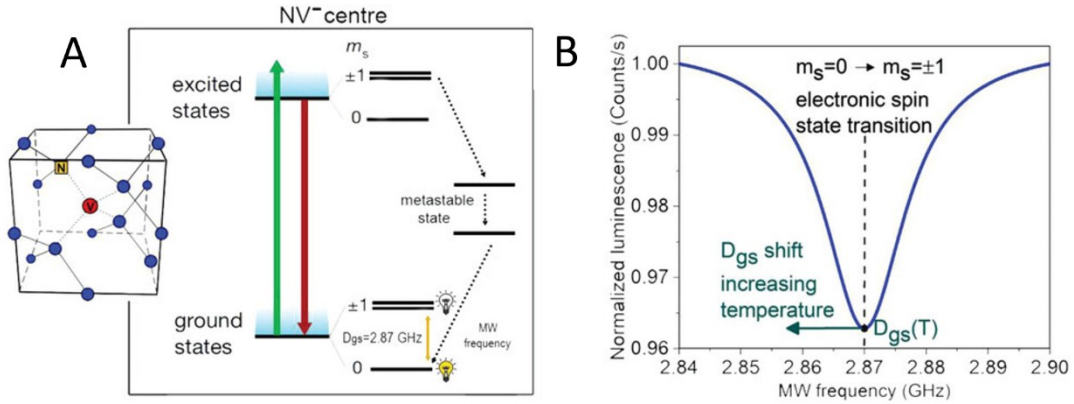

Figure 2: A) NV⁻ charge state electronic structure depicting the transitions responsible for optical readout and spin polarization. B) Dependence of the ODMR resonant frequency on the temperature (Petrini et al., 2022).

1.5.4 Polymer coating & biomedical applications of FNDs

Despite the inherent advantages of FNDs, biomedical applications often require improved physicochemical properties and efficient interaction with biological targets. Surface modifications can achieve this. One of the most common modification strategies is polymer coating. Polymer coating can improve the stability and solubility of FNDs in biological fluids, reducing non-specific interactions and improving their biocompatibility. Another advantage is the introduction of new functional groups onto the FND surface, paving the way for further bioconjugation with, e.g., therapeutic agents, targeting ligands, or imaging probes. The polymer coating can significantly broaden the biomedical applications of FNDs (Qin et al., 2021). Different polymers can be attached to ND's surface in different ways. The main two approaches are non-covalent adsorption *via* electrostatic or hydrophobic interactions and covalent grafting, further divided into “grafting to”, “grafting from”, and “grafting through”.

The electrostatic interaction approach has the advantages of simplicity and versatility. However, the stability of the polymer layer can be lower compared to covalent methods, as it can be influenced by changes in the environment, such as pH and ionic strength. Different cationic polymers, including poly-L-lysine (PLL), polyarginine (PA), and polyethyleneimine (PEI), poly(allylamine hydrochloride) (PAH) have been employed to electrostatically modify the surface of NDs, introducing a high number of primary amino groups. These groups can subsequently form amide bonds with other functional entities via amine chemistry. PEI and PAH

electrostatic coating of NDs was used for the efficient delivery of nucleic acids into the cells (Alhaddad et al., 2011).

The "grafting to" approach is a method that generally involves the reaction of end-functionalized polymers with complementary functional groups on the substrate's surface. On the other hand, the "grafting from" method involves the growth of polymer chains directly from the surface of the substrate. This method generally leads to higher grafting densities compared to the "grafting to" approach, as the polymer chains grow from the ND surface, thereby reducing issues related to steric hindrance. However, the "grafting from" approach often involves more complex chemistry and can require careful control over reaction conditions to ensure successful polymer growth (Neburkova et al., 2017). This method includes atom transfer radical polymerization (ATRP) (Chen et al., 2018) and reversible addition-fragmentation chain transfer (RAFT) polymerization methods (Shi et al., 2015). The “grafting through” approach, also known as the “macromonomer” method, is a technique that begins with the synthesis of a macromonomer - a small polymer with a reactive end group. This macromonomer is then copolymerized with other monomers, which may be small individual monomers or other macromonomers, in a polymerization reaction. Typically, a low molecular weight monomer is radically copolymerized with a (meth)acrylate functionalized macromonomer. The reactive end groups of macromonomer can attach to a ND surface, effectively “grafting” the polymer chains onto the ND surface. This method provides a high level of control over the grafting density, length, and composition of the grafted polymer chains, making it suitable for the synthesis of sophisticated and well-defined architectures (Kim et al., 2022; Yuan et al., 2012).

One of the most studied and extensively used polymers in biological applications is PEG. PEG is usually attached to the ND surface via the “grafting to” approach (Dong et al., 2015; X. Zhang et al., 2012). However, PEGylation of NDs was also done via RAFT polymerization (Shi et al., 2015). PEGylation gained its attraction in NPs modifications mainly due to prolonging circulation time in the bloodstream. This enhanced lifespan within the biological systems allows for improved drug delivery (Mochalin et al. 2015, Wei et al. 2019) or bioimaging (Vaijayanthimala et al. 2009, Zhang et al. 2015). However, it was shown that repeated administration of PEGylated NPs could induce the formation of anti-PEG antibodies in the system, leading to rapid clearance of subsequent doses from the

bloodstream and increasing ND's stability. This phenomenon is known as the "PEG dilemma" (Amoozgar and Yeo, 2012). Moreover, PEGylation can reduce the interaction of NPs with cells which causes reduced cellular uptake and can limit drug delivery or cellular imaging applications (Hu et al., 2018).

Based on mentioned drawbacks, the attention was shifted to other biocompatible polymers. One of the most promising biocompatible polymers is polyglycerol (PG). PG coating is an example of the “grafting from” approach, especially the result of ring-opening polymerization involving glycidol, which initiates at the oxygen-containing functionalities present on the surface of NDs. The hyperbranched polyglycerol layer provides a denser polymer coating compared to linear PEG. The PG layer is characterized by the presence of hydroxyl groups, which confer additional modifiable properties. Consequently, this imbues the PG coating with a greater hydrophilic nature than the PEG coating, which contains ether groups. PG-coated NDs were used in drug delivery in cancer cells (Zhao et al., 2014b), gene delivery (Zhao et al., 2014a), and tumor imaging (Yoshino et al., 2019).

Polydopamine (PDA) is characterized by excellent adhesion to various materials, enhancing interaction with negatively charged cell membranes. PDA coating enhances NDs' stability and provides new functional groups for further modification. PDA-coated NDs were used in photothermal therapy (Maziukiewicz et al., 2019).

Furthermore, a temperature-responsive polymer such as poly(N-isopropyl acrylamide) (PNIPAM) has been studied for its potential in controlled drug release applications due to its interesting responsive behavior (Hu et al., 2019). PNIPAM-coated FNDs are usually prepared using RAFT polymerization and as quantum sensors (Zhang et al., 2018).

Finally, methacrylate derivatives, especially biodegradable and non-immunogenic poly[N-(2-hydroxypropyl) methacrylamide] (PHPMA), were used for polymer coating. This approach is an example of the “grafting through” method. The advantage of the PHPMA coating is the possibility of further side chain modifications if a copolymer is used (Rehor et al., 2014; Slegerova et al., 2015).

In summary, a broad spectrum of biocompatible polymers has been investigated for their potential in FND coating (Figure 3). The primary motivation for this is the capacity of these polymers to enhance the properties of FNDs, thereby making them more suitable for biomedical applications, mainly for bioimaging, drug

delivery, and tissue engineering. The selection of the polymer for the coating is application-dependent, and the desired properties of the final FND-polymer conjugate guide it.

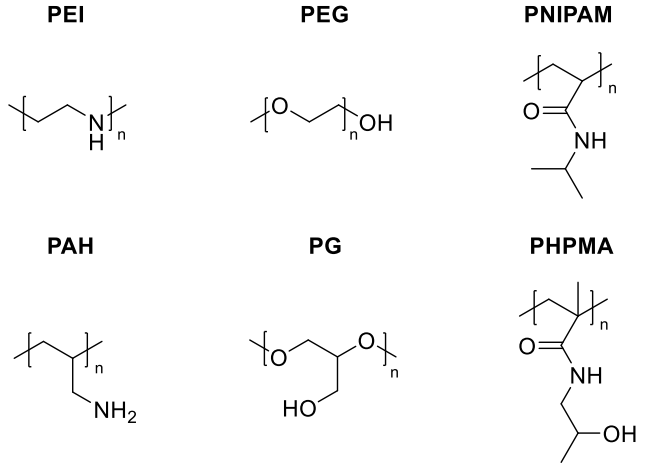

Figure 3: Examples of polymer structures used for ND coating.

1.6 Gold nanoclusters

Gold nanoclusters (AuNCs) are composed of a few to several dozen gold atoms, and their size is usually less than 2 nm. They have attracted significant attention over the past few decades due to their unique optical, electronic, and catalytic properties, attributed mainly to their quantum size effects and the consequent discrete electronic structure. AuNCs possess interesting size-dependent optical properties and are generally nontoxic (Zhang et al., 2014). AuNCs can have distinct absorption and photoluminescence (PL) features, often covering a wide range of visible and near-infrared regions. This luminescence behavior and their excellent photostability make them appealing candidates for various optical applications (Zhou et al., 2019).

1.6.1 Biocompatibility of AuNCs

AuNCs are considered nontoxic based on the inertness of gold. Gold is a noble metal that is highly unreactive, which prevents AuNCs from being harmful in biological systems. Gold is also biocompatible material; therefore, it does not trigger an immune response or cause other adverse biological effects (Kadhim et al., 2021). However, NP toxicity is size-dependent, therefore, bigger gold nanoparticles (AuNPs) can show accumulation in the liver and spleen and, due to their poor degradation, can induce acute toxicity (Blanco et al., 2015; Ehlerding et al., 2016). Luckily, AuNCs can be coated or functionalized with various biocompatible

substances to increase their stability in biological environments and reduce their interaction with proteins and cells, which could otherwise lead to toxicity and change in their biodistribution. Moreover, gold nanoclusters' size and shape can be controlled during the synthetic process, which helps to avoid sizes or shapes that could be toxic (Kumar et al., 2023; Kumar, 2009).

1.6.2 Size and optical properties of AuNCs

The optical properties of various NPs exhibit a correlation with their size. Ultrasmall (<2 nm) gold nanoclusters (AuNCs), situated at the intersection between individual atoms and NPs, exhibit unique properties distinctly different from their macroscopic or atomic counterparts. These properties are mainly attributable to quantum size effects, which cause the optical characteristics of AuNCs to be heavily dependent on their size (Huang et al., 2018).

One of the most attractive optical properties of AuNCs is their size-dependent absorption and emission spectra. As the size of the gold particles diminishes to a few nanometers, AuNCs contain only a few atoms, resulting in a restriction on the motion of electrons which, in contrast, can move freely throughout bulk gold. This confinement quantizes energy levels, establishing discrete energy states that the electrons can occupy, which indicates molecular-like behavior and not metal-like behavior. Thus, AuNCs display distinct absorption peaks, in contrast with the broad surface plasmon resonance (SPR) observed in larger AuNPs of size 3-100 nm (Huang et al., 2018; Zhang et al., 2014; Zhou et al., 2019).

The cluster size directly influences the positioning and intensity of these absorption peaks, as the energy spacing between electronic states changes with the size of the cluster. Smaller clusters typically exhibit a larger energy between the highest occupied molecular orbital and the lowest unoccupied molecular orbital (HOMO-LUMO gap), which results in a blue shift of the absorption spectra (Kwak et al., 2017). Consequently, the emission spectra of AuNCs also display size dependency. The emission spectra originate from the radiative recombination of electron-hole pairs, which involves an electron transitioning from the LUMO to the HOMO band, subsequently releasing energy as light. Alterations in cluster size modify the energy state spacing and, subsequently, the emission wavelength. A decrease in size generally induces a red-shift in the emission peak (Yang et al., 2021).

The quantum yield, a measure of PL efficiency, is yet another optical property of AuNCs strongly influenced by their size. Smaller AuNCs tend to have higher quantum yields, mainly due to the suppression of nonradiative relaxation pathways. With a larger energy gap between the ground and excited states, smaller AuNCs experience less nonradiative decay. Additionally, the limited size reduces the number of vibrational modes available for nonradiative relaxation, thereby increasing the probability of radiative recombination and enhancing the quantum yield. These properties make AuNCs promising materials for applications in bioimaging and optoelectronics (Luo et al., 2023).

The fluorescence lifetime of AuNCs has also been an active area of research. AuNCs show a long fluorescence lifetime (μs), and this longevity is also attributed to mentioned molecular-like behavior, especially to quantum confinement and minimized nonradiative decay pathways. In combination with good stability, AuNCs maintain their long fluorescence lifetime even in biological systems (Hada et al., 2021).

The specific photoluminescent properties of AuNCs, such as the wavelength of emitted light, can be significantly influenced by other factors, such as the type of ligands stabilizing the cluster and the specific arrangement of the gold atoms within the cluster. These factors can impact the energy levels and transitions that the electrons can undergo, thus influencing the characteristics of the emitted light (Jin et al., 2016). However, the correlation between the structure of AuNCs and their optical properties is still not completely understood (Huang et al., 2018).

1.6.3 Modifications of AuNCs

AuNCs are frequently synthesized with a surface monolayer of ligands to protect the Au core. NIR photoluminescent AuNCs are typically stabilized by surface ligands such as thiolates because they provide excellent stability to the Au core (Häkkinen, 2012). Thiol groups bond to Au via metal-thiolate bond, which is a type of covalent bond. Different thiol-containing ligands were used for the Au core stabilization, such as lipoic acid (Mishra et al., 2016), mercapto succinic acid (Muhammed et al., 2010), 11-mercaptoundecanoic acid (Wei et al., 2021), thiolated polymers (Oh et al., 2013) and also small biomolecules like glutathione (GSH) (Stamplecoskie and Kamat, 2014). The type, density, chain length, and arrangement of ligands can significantly impact the size, stability, and solubility of AuNC but also

the optoelectronic properties of the AuNCs (Pramanik et al., 2018). Besides small molecules, proteins such as bovine serum albumin (BSA) are often used as capping ligands to synthesize stable photoluminescent AuNCs (Chen et al., 2015). BSA is a large protein containing many amino acids, including cysteine. Cysteine residues can form covalent bond with gold, and other residues can interact with the gold surface *via* weaker, non-covalent interactions (like van der Waals forces, hydrogen bonds, or electrostatic interactions), this process is called passive adsorption. The larger size and complex structure of BSA can allow it to create a dense coating around the gold nanocluster (Bolaños et al., 2019).

The strong bond between gold and sulfur (Au-S) atoms can help suppress nonradiative decay pathways by stabilizing the electronic structure of the AuNCs. This stabilization minimizes the availability of vibrational modes that can lead to nonradiative decay, thus favoring radiative (light-emitting) relaxation pathways and enhancing the quantum yield. Moreover, the sulfur-containing ligands can tune AuNCs absorption and emission spectra, thus enhancing the quantum yield. The Au-S bond also protects the quantum states of the electrons in the AuNCs and can help maintain the quantum yield of the AuNCs (Li et al. 2022).

In addition to stabilizing AuNCs and tuning their optoelectronic properties, surface modifications can also introduce new functional groups to the cluster surface. These newly introduced functionalities enable targeted delivery and open new avenues for the use of AuNCs in biomedical applications (Shenoy et al., 2006).

Doping AuNCs with heteroatoms is another approach for fine-tuning their properties. Doping adjusts the electronic structure of the AuNCs, which tailors their catalytic and optical properties. For instance, doping AuNCs with atoms like Ag, Pd, Pt, or Cu has been shown to enhance their catalytic activity toward specific reactions. In some cases, doping also leads to size (Qian et al., 2012) and shape control, further influencing the physical and chemical behavior of the clusters (Zhou et al., 2015). It was shown that doping by the precise number of Ag atoms increases AuNCs quantum yield, however, it is experimentally challenging (Wang et al., 2014).

Post-synthetic treatments, for example, etching, can further tailor the properties of AuNCs. Chemical etching can reduce the nanoclusters' size, thereby tuning their quantum confinement effects (Wei et al., 2021).

1.6.4 Biomedical applications of AuNCs

In biomedicine, AuNCs have shown great promise as robust agents for biolabeling, bioimaging, and theranostics. Moreover, their potential in photothermal therapy and photodynamic therapy underscores their relevance to modern medicine. Various AuNC-based systems were developed for these specific applications (Zheng et al., 2017).

First-time prepared NIR emitting AuNCs were stabilized by BSA with quantum yield approx. 6 % (Xie et al., 2009). However, further investigation found that BSA-AuNCs have poor colloidal stability and biodistribution (X.-D. Zhang et al., 2012). BSA is still the most commonly used protein because it is a stabilizer and reducing agent during AuNC synthesis. BSA-stabilized AuNCs were applied in various *in vivo* applications (Porret et al., 2020). BSA-AuNCs were also modified by targeting molecules to enhance the accumulation of the BSA-AuNCs in tumors. Several (bio)molecules were used for active tumor targeting, for example, folic acid targeting folate receptors (Zheng et al., 2012), and hyaluronic acid targeting receptors CD44, both receptors are overexpressed in cancer cells (Zhang et al., 2014).

GSH gained attention and has been used for AuNc modification because it also plays the role of stabilizer and reducing agent. GSH shows limited interaction with cellular proteins. Moreover, it reduces the accumulation of AuNCs in the liver and spleen and increases clearance (Zhou et al., 2012). Another advantage of GSH capping is strong fluorescence enhancement (Yahia-Ammar et al., 2016). Therefore, various GSH-capped AuNCs with long-living NIR emission were synthesized and could be potentially used *in vitro* or *in vivo* (Hada et al., 2021; Li et al., 2020; Shang and Nienhaus, 2012). Folic acid was also used as a tumor-targeting molecule in the case of GSH-AuNC, and the resulting conjugate was used in (computed tomography) CT imaging of gastric cancer (Zhou et al., 2013). Other proteins, including trypsin (try), were used for AuNC modification. Active tumor targeting via folic acid conjugated try-AuNCs was employed for *in vivo* imaging in mice and successful tumor imaging (Liu et al., 2013).

While proteins and small biomolecules have been widely utilized for AuNc stabilization, the research moved toward the employment of synthetic polymers providing higher control over physical and chemical properties. For example, AuNC-containing PEGylated moieties were evaluated *in vitro* for possible applications

in mice's NIR image-guided surgery of head and neck tumors (Colombé et al., 2019). PEG and thermoresponsive NIPAM were also used for micelle formation as AuNC stabilizers, and these systems were investigated as promising tool in laser-guided drug release therapies (Hebels et al., 2021).

AuNCs functionalized with gadolinium were usually used for magnetic resonance imaging (MRI) and were also investigated for dual imaging, including MRI and CT imaging (Hembury et al., 2015). Later, AuNC based system for triple-modal imaging *in vivo* was developed. This AuNCs-based Gd system exhibits a significant boost in signals for NIR-fluorescence imaging, CT, and MRI. The mentioned *in vitro* observations were confirmed in tumor-bearing mice. Gadolinium nanoclusters were preferentially accumulated in tumors and showed quick renal clearance (Hu et al., 2013).

In conclusion, AuNCs present a versatile platform with wide-ranging potential applications in biomedicine. From diagnostics and therapy to biosensing, their unique properties open up numerous possibilities for their use in addressing critical challenges in healthcare.

1.7 Visualization of sentinel lymph nodes

1.7.1 Histology of sentinel lymph nodes

Lymph nodes (LNs) are vital immune system components and are small, bean-shaped lymphatic system structures distributed throughout the body. Their function is to filter and eliminate foreign substances from the lymph, a fluid that contains immune cells and waste products (Murphy and Weaver, 2016).

Sentinel lymph nodes (SLNs) are the first LNs to which cancer cells spread from the primary tumor. Therefore, the histological analysis of SLNs is critical for correct cancer staging and adjustment of the treatment plan. SLNs are typically located near the primary tumor and are identified by their drainage patterns (Lambrou and Amadeo, 2021). Histologically, LNs can be divided into three main regions: the cortex, paracortex, and medulla. The cortex consists of lymphoid follicles containing germinal centers, where B-cells undergo maturation, proliferation, and differentiation. The paracortex contains T-cells and high endothelial venules, facilitating the entry of lymphocytes and antigen-presenting cells. Lastly, the medulla comprises medullary cords and sinuses, serving

as a pathway for lymph flow and allowing the interaction of immune cells with antigens (Murphy and Weaver, 2016).

1.7.2 Detection of sentinel lymph nodes

Observations on SLNs were done first by Gould (1960) and his colleagues on cancer of the parotid. However, 30 years later, Morton (1992) and his colleagues were the first to describe the concept of lymphatic mapping while working on intraoperative sentinel LN visualization in early-stage melanoma in breast cancer. They observed migration of peritumoral injected dye to sentinel LNs, allowing visual identification and their removal for biopsy. Krag (1993) and Giuliano (1994), with their colleagues, later approved Morton's procedure, and further, it was validated by Turner et al. (1997), Giuliano et al. (2000), and Haigh et al. (1999). Their development of this technique resulted in the general acceptance of sentinel LN mapping, and today it is the standard of care primarily for breast cancer (Chatterjee et al., 2015) and melanoma patients (Ferri et al., 2021), and it is a prospective method for colon cancer treatment (Ankersmit et al., 2019).

SLN accurate detection is crucial before the sentinel lymph node biopsy (SLNB) can be done. The primary goal of SLNB is to determine whether metastasis has occurred, allowing for proper cancer staging and guiding treatment decisions. A negative SLN result indicates that cancer has not spread to the lymphatic system, and the patient may avoid more extensive LN dissection, reducing the risk of complications such as lymphedema. In contrast, a positive SLN result signifies the presence of metastasis, necessitating further treatment such as adjuvant therapy complete LN dissection. The SLN is a crucial prognostic factor in cancer treatment and can influence long-term patient outcomes (Krag et al., 2010; Morton et al., 2006; Veronesi et al., 2010).

Various methods were established to detect SLNs, the first method was blue dye injection. In this method, a blue dye is injected into the area surrounding the primary tumor, which then travels through the lymphatic vessels to the SLNs. The SLNs are then identified by their blue color and removed during the surgery. The main drawback of this method is that the blue dye is not easily visible through the skin or tissues. SLN detection is inaccurate and strongly depends on the surgeon's experience, however, the method is technically simple therefore, commonly used (Ang et al., 2014); Moreover, the risk of allergic reaction to blue dyes

(Krag et al., 2007) and fat necrosis (Piscatelli et al., 2009) were also described. These limitations led to the development of alternative methods for SLN detection in SLNB, such as the use of radioactive tracers (lymphoscintigraphy).

In addition, techniques using radioisotopes were employed in SLN mapping. Lymphoscintigraphy is a preoperative non-invasive technique involving injecting a radioactive tracer into the area surrounding the primary tumor. The tracer travels through the lymphatic vessels to the SLNs, which are then detected using a gamma camera. This method is performed preoperatively. Gamma probe detection also involves a radioactive tracer, like in the case of lymphoscintigraphy. However, this technique is intraoperative, and the handheld gamma probe guides the surgeon to the SLNs (Mettler and Guiberteau, 2019). Radioactive tracers show many advantages over blue dyes, but patients and caregivers are exposed to ionizing radiation during the operation. Another drawback is that the procedure is costly and has a poor spatial and temporal resolution in imaging (Vahrmeijer et al., 2013).

Among NIR-emitting fluorescent dyes, ICG was used the most for SLN detection (Figure 4). ICG application showed several advantages over common blue dyes and radiocolloids, such as real-time imaging, allowing for immediate lymphatic drainage patterns detection and dynamic SLN visualization during surgery. ICG provides NIR emission; therefore, a high signal-to-noise ratio and precise SLN identification are achieved (Sugie et al., 2017).

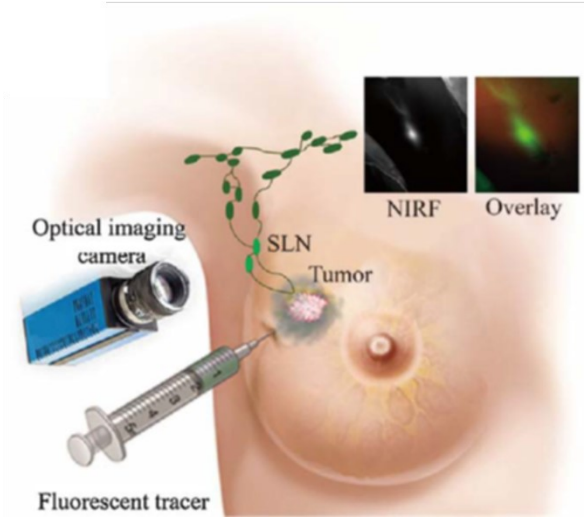

Figure 4: Scheme of sentinel lymph node visualization using fluorescence. Reproduced and adapted from the literature (Qiu et al. 2017).

Combined methods involving both a radioactive tracer and a blue dye were investigated for more accurate SLN detection (Ahmed et al., 2014). In addition, combining radioactive tracers with fluorescent dyes (ICG) was described and showed superior detection to common blue dyes (Deken et al., 2020). However, none of these techniques solve the problem of avoiding ionizing radiation altogether. Therefore, more advanced methods have been developed today, such as magnetic tracers (Teshome et al., 2016) or advanced fluorescent probes (Yue et al., 2018).

The magnetic tracer method uses the magnetic tracer, which is injected peritumorally, and subsequently, the SLN is localized by and handheld magnetometer. Pouw (2015) and his colleagues showed that the magnetic tracer method is effective and can be used for preoperative imaging using MRI and intraoperative SLNB. However, magnetic tracers also have limitations, such as the risk of allergic reactions to iron, possible skin discoloration, and pigmentation. Furthermore, metal instruments are forbidden during operation to avoid interference with the magnetometer (Sreedhar et al., 2021). A few years ago, (Kuwahata et al., 2020) and colleagues came up with the idea to combine a magnetic tracer with ICG, and they identified SLNs in mice. The detection of SLN was more accurate than ICG visualization or using magnetic tracers separately and could have future potential.

1.7.3 Fluorescence-guided surgery

Despite the enormous effort and recent advantages in preoperative and intraoperative techniques, surgical margin (cut edge of a surgical specimen) positivity did not change significantly over the last few decades. These limitations can be overcome by employing Fluorescence-guided surgery as a promising technique to identify tumor and surgical margins more accurately (Nagaya et al., 2017).

Fluorescence-guided surgery (FGS) has emerged as an innovative technique that harnesses the power of fluorescence imaging to improve surgical precision, patient outcomes, and healthcare efficiency. FGS provides improved intraoperative visualization, thus becoming particularly beneficial in oncological surgeries, which is critical to achieving complete tumor resection while sparing healthy tissues. The fundamental concept behind FGS is the utilization of fluorescent dyes, which are administered to the patient either systemically or locally. These dyes accumulate

preferentially in cancer cells or tissues and emit fluorescence when illuminated with light of a specific wavelength. This fluorescence can be detected using specialized imaging equipment, such as a fluorescence camera, providing real-time visualization of cancer cells and tissues (Vahrmeijer et al., 2013). This technique can overcome weak fluorescence signals and penetration depth. The camera output is usually displayed on a monitor, including a merged image of the fluorescence signal and the white light image (Nagaya et al., 2017).

Several NIR-emitting dyes were used in FGS for cancer treatment, such as ICG (Vahrmeijer et al., 2013; Van Manen et al., 2018), and IRDye 800CW (Wellens et al., 2020). Furthermore, 5-Aminolevulinic acid (5-ALA), a prodrug converted into fluorescent molecules by tumor cells, has also been used in FGS for cancer treatment (Stummer et al., 2006). Therefore, FGS has been used successfully in various cancers, including breast (Kuehn et al., 2013; Sugie et al., 2017), gastric (Namikawa, 2015), colorectal (Cahill et al. 2012), and melanoma (Sugie et al., 2017) FGS has also been used in neurosurgery (Acerbi et al., 2013) and urology (Tobis et al., 2011). The clinical applications of FGS are numerous and expanding rapidly. One of the most promising applications is cancer-containing SLN detection because using FGS enables the detection of small tumors and metastases that are difficult to detect using conventional imaging methods. FGS can be used to identify the location of SLNs more accurately, reducing the risk of positive margins and damage of nearby tissues, blood vessels, and organs (Nagaya et al., 2017).

2 AIMS OF THE THESIS

The main objective of this thesis is to prepare new types of biocompatible NIR-emitting fluorescent probes and evaluate their potential for biomedical applications.

The following specific aims were proposed to answer the hypotheses:

- Hypothesis: Is it possible for FNDs to exhibit biocompatibility and high-brightness as *in vivo* fluorescent probes?

  Experimental approach: To develop a preparation of ultrabright FNDs equipped with a biocompatible interface and evaluate their colloidal stability.

- Hypothesis: Can mannose facilitate the uptake of mannose-labeled FNDs by macrophages in SLNs?

  Experimental approach: Functionalize the biocompatible polymer layer on FNDs and covalently attach mannose. To evaluate the mannose targeting of FNDs *in vitro* and *in vivo*.

- Hypothesis: Can FNDs be used as intracellular nanothermometers?

  Experimental approach: To design and prepare FNDs with narrow size distribution suitable for nano thermometry. To demonstrate temperature measurement *in vitro*.

- Hypothesis: Can gold nanoclusters be used as cellular fluorescent probes?

  Experimental approach: To develop a new synthetic approach with high control over the photophysical properties of AuNCs and to evaluate their performance *in vitro*.

- Hypothesis: Can the optical performance of AuNCs be further boosted at the nanoscale level?

  Experimental approach: To design and synthesize tunable plasmonic nanosystems enhancing the emission of AuNCs.

3 METHODS

All the methods used in this Ph.D. thesis are summarized in this chapter. Detailed information about the methods can be found in previously listed related publications.

Methods used in this thesis were as follows:

Synthetic and material chemistry methods

Synthesis of α-D-mannose-PEG3-azide, ND irradiation, ND oxidation, polyglycerol coating, copper-catalyzed azide-alkyne cycloaddition, synthesis of gold nanoclusters, synthesis of gold nanorods, synthesis of complexes of gold nanoclusters with gold nanorods.

Physico-chemical methods

Dynamic light scattering (DLS), electron microscopy, thermogravimetry, size fractionation, Fourier-transformed infrared spectroscopy, fluorescence spectroscopy, optical spectroscopy, spectrophotometry, optically detected magnetic resonance, flow cytometry, confocal microscopy (fluorescence), CHN analysis, inductively coupled plasma optical emission spectroscopy, nuclear magnetic resonance, electrospray ionization mass spectrometry, transient absorption spectroscopy, X-Ray photoelectron spectroscopy, neutron activation analysis.

***In vitro* and *in vivo* experiments**

Cell culture experiments, cell viability assays, FND internalization imaging, live cell imaging, *in vivo* imaging, and histological analysis of SLNs.

Statistical methods

One-way ANOVA - Dunnett's test, two-way ANOVA - Tukey's test, Welch t-student test.

4 SUMMARY OF THE RESULTS AND DISCUSSION

This work presents an extensive study on the preparation, modification, and utilization of FNDs and AuNCs as promising nanoprobes for biomedical applications, emphasizing bioimaging. These nano-sized probes exhibit emission in the near-infrared region, the optimal range for bioimaging.

In the first part of our study, we optimized the synthesis of biocompatible, photostable, and colloidally stable mannose-containing polymer-coated FNDs (FND-p-Man). *In vitro* experiments confirmed no cytotoxic effects and showed enhanced uptake of FND-p-Man. We observed that the mannose receptor plays a crucial role in the internalization of mannose-containing FNDs. FND-p-Man showed enhanced retention in the mice SLNs *in vivo*. Therefore, FND-p-Man may serve as a promising tracer in endoscopic/robotic fluorescence-guided surgeries (Kvakova et al., 2022).

In addition, we employed unique FND properties for temperature sensing *in vitro*. Specifically, ODMR was used to measure temperature variations in hippocampal neurons. A significant correlation between altered neuron firing activity and temperature change was observed at the single-cell level using the FND-based nanosensors (Petrini et al., 2022).

In the second part, we developed a facile synthesis of near-infrared photoluminescent AuNCs stabilized with thioctic acid and thiol-terminated PEG, further modified with 3-(aminopropyl) triphenylphosphonium (TPP) bromide. Resulting AuNCs exhibit increased PL upon TPP attachment and stable emission. Confocal imaging of HeLa cells incubated with the functionalized AuNCs demonstrated successful cellular uptake of the AuNCs, confirming their potential for use in biological imaging applications (Pramanik et al., 2020).

Since we aim to utilize AuNCs in bioimaging, their optical properties were thoroughly investigated. AuNCs exhibit robustness against photo-degradation and favorable spectral characteristics, particularly within the biological imaging window, providing significant advantages for biological applications. It was also shown that the PL intensity declines to a stable level upon strong excitation, potentially due to AuNCs' heating, enabling nano thermometry (Valenta et al., 2021).

As previously shown, capping ligands strongly influence the optical properties of AuNCs, which motivated us to functionalize the stabilized thioctic acid, PEG-containing AuNCs, further. Heavy atom (iodine) functionalized AuNCs revealed a rare inverse heavy atom effect (HAE) - a phenomenon that enhances the long-lived triplet excited lifetime of AuNCs. This property of iodine-functionalized AuNC can also be beneficial in bioimaging applications (Pramanik et al., 2021).

The final part of our study introduces a novel method using silica shells on gold nanorods (AuNRs) to attach TPP-AuNCs for the preparation AuNRs@AuNCs. The study demonstrates that PL intensity enhancement is maximized by tuning the number of attached AuNCs and matching the excitation wavelength to the AuNRs' plasmonic band. The greatest enhancement was observed with a 5 nm silica shell at 633 nm excitation (Pavelka et al., 2022). The findings also underscore the importance of separation distance and AuNCs positioning on AuNRs surfaces in photoluminescence – localized surface plasmon resonance (PL-LSPR) coupling and suggest potential emission enhancement *via* increasing the AuNR volume (Pavelka et al., 2023).

4.1 Visualization of Sentinel Lymph Nodes with Mannosylated Fluorescent Nanodiamonds

Kvakova, K.; Ondra, M.; Schimer, J.; Petrik, M.; Novy, Z.; Raabova, H.; Hajduch, M.; Cigler, P.

Although there has been extensive research on ≈100 nm FNDs for advanced *in vivo* imaging, their limited brightness and signal-to-noise ratio restrict their widespread utilization (Igarashi et al., 2012; Vaijayanthimala et al., 2012; Wu et al., 2013). Existing methods to enhance brightness require complex instrumentation and thus are not routinely available (Chapman and Plakhoitnik, 2013). In our work, we propose a solution using ≈200 nm HPHT FNDs. The bigger FND volume also increases the number of NV centers and decreases surface influence, resulting in higher brightness necessary for bioimaging. These FNDs have two-color emission (excitation-dependent) caused by the presence of NV^- centers (red) and NVN centers (green) (Dei Cas et al., 2019) (Figure 5A).

Initially, a narrow size fraction of NDs was separated, subsequently irradiated, annealed, and oxidized (Figure 5B) to yield ultrabright two-colored FNDs. "Naked" FNDs suffer from poor colloidal stability in buffers and biological fluids (Slegerova et al., 2015; Wilson et al., 2019). Moreover, non-specific protein interactions could be problematic. Therefore, polymer coating was employed to overcome these problems (Neburkova et al., 2017).

To achieve effective polymer coating, we employed a densely packed hyperbranched polyglycerol layer. This coating ensures not only strong steric colloidal stabilization but also provides excellent antifouling properties, leading to prolonged circulation in the bloodstream (Neburkova et al., 2017). PG layer was grown from the surface of oxidized, negatively charged FNDs *via* ring-opening polymerization of glycidol at 130 °C. Subsequent copolymerization with glycidyl propargyl ether (Barton et al., 2020; Hsieh et al., 2019) introduced alkyne groups to the PG shell, yielding a biocompatible colloidally extremely stable FND-p (Figure 5B) sample suitable for bioorthogonal modifications. Other polymerization approaches suitable for smaller FND particles proved inefficient/inappropriate for ≈200-nm FNDs, (for example, silica-coated methacrylate-modified FNDs) (Neburkova et al., 2018b, 2018a; Slegerova et al., 2015). The FND-p sample was further modified using bioconjugation techniques, resulting in colloidally stable

mannose-modified FND-p-Man (Figure 5B). The stability of the prepared FND-p and FND-p-Man was tested in a high-ionic environment. DLS data showed improved stability of FNDs after polymer coating, and the stability remained unchanged after mannosylation (Figure 5B).

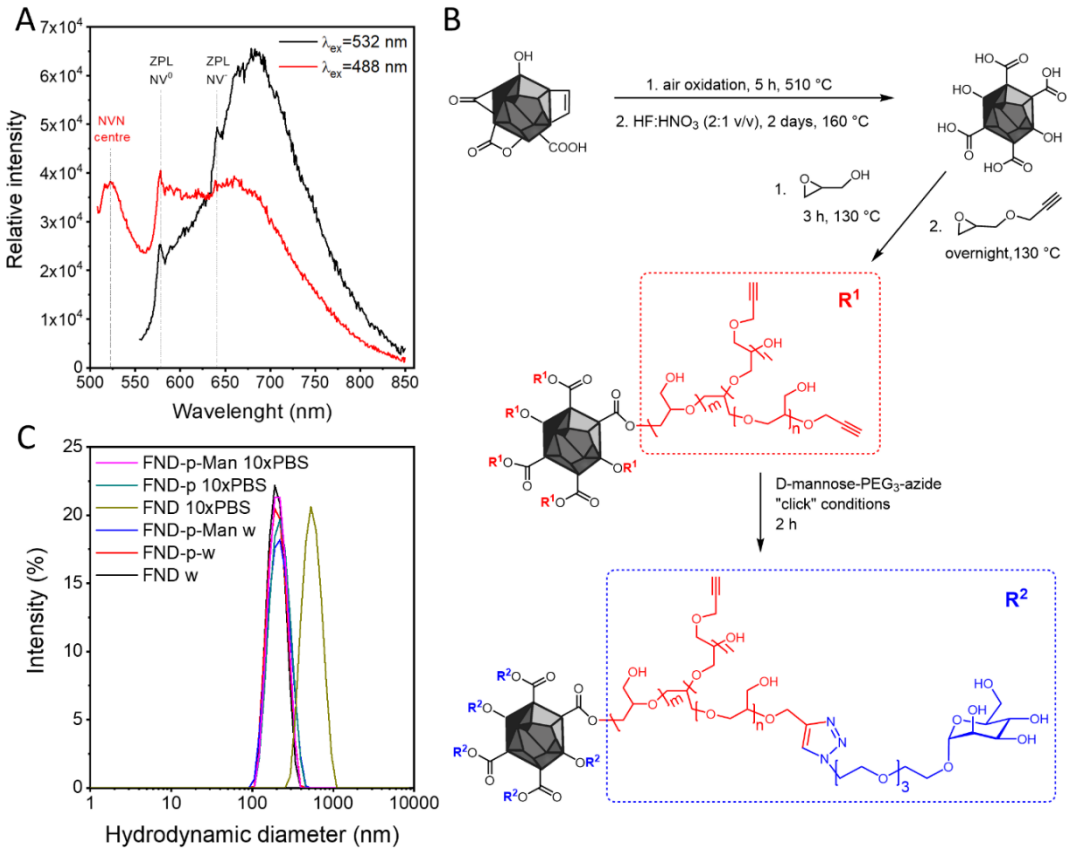

Figure 5: A) The PL spectra of FNDs illustrate both NV and NVN centers presence, excitation wavelengths 532 and 488 nm. B) Preparation of FND, FND-p, and FND-p-Man. C) Comparison ofcolloidal stabilities of prepared FNDs. DLS results showed improved stability of FND-p and FND-p -Man compared to FND in a highly ionic environment (10x PBS).

Later, we assessed the cytotoxicity of FND-p and FND-p-Man using the cell viability (MTS) assay on J774A.1 mouse macrophage tumor cells. These cells were selected due to their variable surface expression of functional MR, mirroring MR expression in various types of macrophages in LNs. No significant effect on cell viability was observed with FND-p/FND-p-Man concentrations of 5–200 µg/mL after 24 hours, confirming FND non-cytotoxicity (data shown in the publication, Fig. 2). Confocal fluorescence microscopy was then employed to examine FND-p uptake and the effect of mannosylation on FND-p-Man internalization. After 24 hours of treatment, an evident increase in FND-p-Man internalization was observed compared to FND-p (Figure 6). Two-color emission of FND-p-Man was visible after

internalization and accumulation upon excitation with two different lasers, demonstrating the potential of these particles in live imaging (data shown in the publication, Fig. 2).

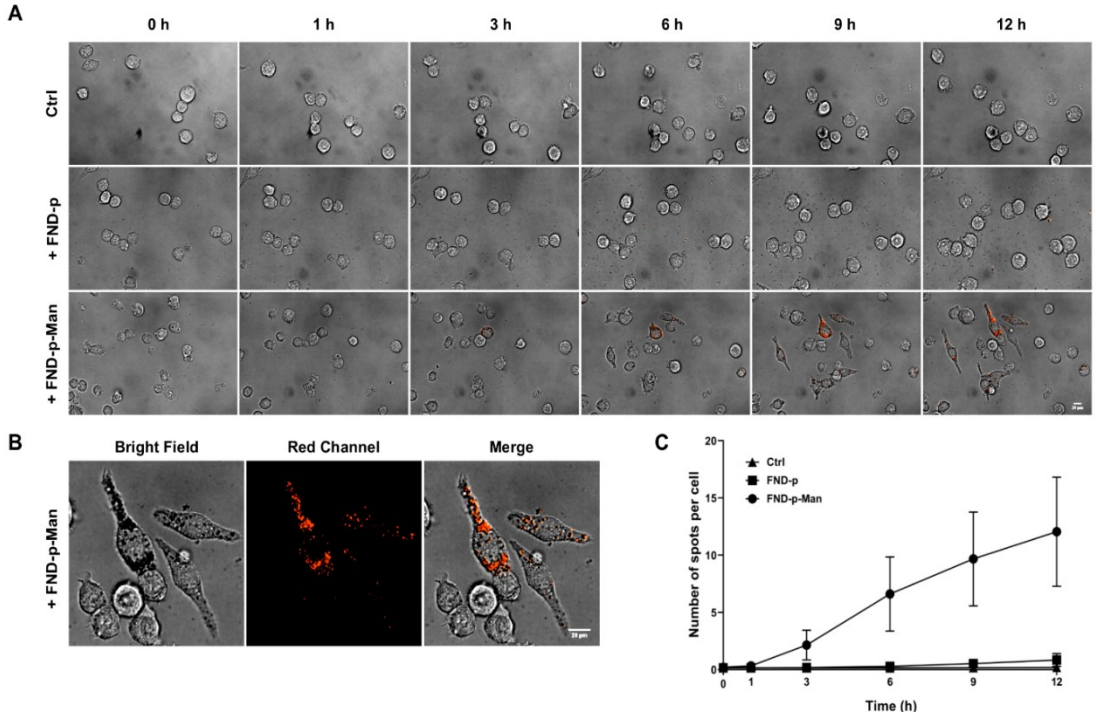

Figure 6: Uptake of FND-p and FND-p-Man into J774A.1 cells. A) Live-cell imaging, merging bright field and red channels, illustrating the internalization of FND-p and FND-p-Man (10 µg ml^{-1} each). B) The distribution of FND-p-Man within J774A.1 cells, as observed after a 12-hour period. C) Quantitative analysis depicting the average count of spots per cell (mean ± standard deviation) following NP uptake over a temporal gradient; n = 3. Scale indicators: In panels A) and B), the scale bars correspond to 20 µm.

Monosaccharides and branched sugars (oligosaccharides, polysaccharides) are known to bind mannose receptor (MR, CD206). The branched sugars bind to MR more effectively and can be used as competitive inhibitors for MR (Taylor and Drickamer, 1993). Another approach to inhibit MR function is the usage of neutralizing antibodies (Verbij et al., 2017). Therefore, to confirm the role of the mannose on FND-p uptake, an inhibition assay was designed to demonstrate the internalization of FND-p-Man via MR. The application of the mannose analog (mannan) and the neutralizing 15.2 mAb significantly reduced the number of spots per cell during live-cell imaging, suggesting MR-mediated internalization. This result was confirmed by experiments on four different epithelial cell lines (16HBE14o-, A549, HCT116, HEK293T) lacking MR expression (Dos Santos et al., 2011;

Kuhn et al., 2014). Minimal or no internalization of FND-p-Man was observed in these cell lines, further confirming the specific involvement of MR in FND-p-Man internalization (data shown in the publication, Figure S5).

To assess the utility of FNDs as NIR fluorescence imaging tracers for SLN imaging, an *in vivo* mouse model was used. FNDs were tested for lymph drainage from the mouse footpad to the regional LNs. The accumulation of both FND-p-Man and FND-p in popliteal LNs following injection showed higher fluorescence signal intensities compared to controls, demonstrating better contrast with FND-p-Man. Further, a murine footpad melanoma model (B16-F10 cell lime) (David Nathanson et al., 1997; Harrell et al., 2007; Servais et al., 2011) was used to assess FNDs' effectiveness in tumor contexts. Necropsy revealed more intense fluorescence in experimental nodes, confirming the preferential uptake of FND-p-Man in SLNs. Importantly, there was no evidence of FND-p-Man distribution outside the administration site and regional LNs, indicating localized targeting (Figure 7).

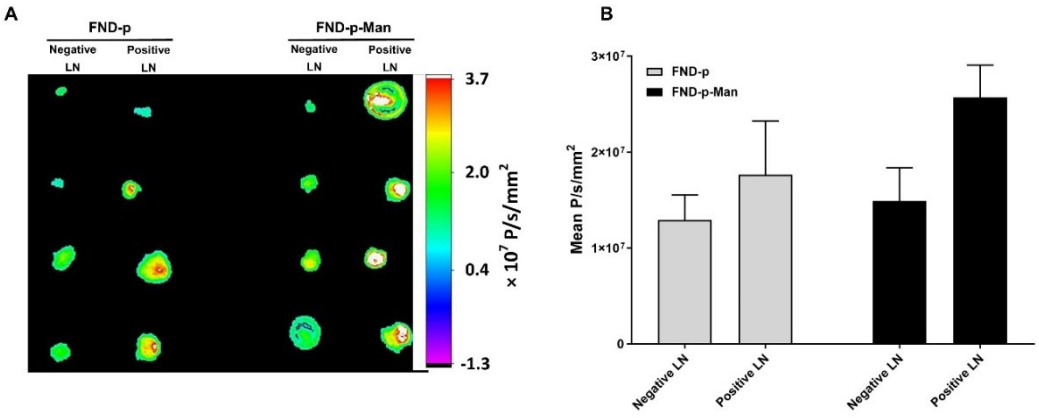

*Figure 7: A) Fluorescence images of four B16-F10 tumor-bearing animals popliteal LNs excised 24 p.i., The comparison between negative LNs and positive LNs (injected with either FND-p or FND-p-Man). B) Statistical representation of the fluorescence intensity signifies the accumulation of FND-p or FND-p-Man in the excised popliteal LNs (mean ± SD, n = 4). P-values were derived through an unpaired two-tailed Student's t-test; ns stands for non-significant, while **p represents a significance level less than 0.005.*

Histological analysis of LNs is crucial to pinpoint sites for the uptake of lymph antigens. LNs, composed of the cortex, paracortex, and medulla compartments, contain different immune cells (Girard et al., 2012; Trevaskis et al., 2015). Subcapsular sinus macrophages are abundant in LNs, and pivotal in surveillance and response (Gray and Cyster, 2012; Louie and Liao, 2019; Moran et al., 2019). In order to ascertain and identify the site of FND retention, we analyzed

LNs from tumor-bearing animals injected with either FND-p or FND-p-Man. Light microscopy revealed the presence of FNDs as dark spots, primarily in the LN subcapsular sinus, with no dark spots in control LNs. A higher number and larger dark spots were observed in animals injected with FND-p-Man compared to those with FND-p, suggesting superior retention of FND-p-Man (Figure 8). This observation was consistent with *in vivo* imaging results and indicated that the accumulation of FNDs in SLNs did not trigger a local inflammatory response.

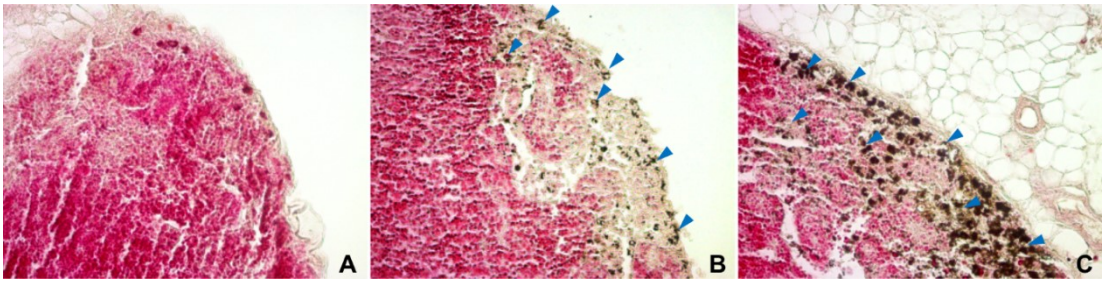

Figure 8: Exemplary images of experimental popliteal LNs removed 24 hours post-injection from animals with tumors. A) Displays a negative control, B) features an animal injected with FND-p, and C) shows an animal injected with FND-p-Man. These are light microscopy images captured with a 20× magnification objective. LNs underwent counter-staining with neutral red; blue arrows indicate the accumulation of FND-p or FND-p-Man in the subcapsular sinus; n equals 4. There was no observed sign of an inflammatory response due to NP accumulation in the SLNs.

Given the findings from our study, we posit that FND-p-Man holds considerable potential as a tracer for sentinel LNs in endoscopic or robotic fluorescence-guided surgical procedures. Furthermore, its broader biomedical applications will appear promising in the forthcoming years.

My contribution:

I oxidized FNDs, separated them by size, optimized their bio-compatibilization – polyglycerol coating, and conducted further surface modifications using bioconjugation techniques. Moreover, I characterized the samples (DLS, spectroscopy) and evaluated their stability. I was involved in the experiment design (including the biological experiments), analyses, and interpretation of data, and I significantly contributed to the manuscript preparation.

4.2 Nanodiamond–Quantum Sensors Reveal Temperature Variation Associated to Hippocampal Neurons Firing

Petrini, G.; Tomagra, G.; Bernardi, E.; Moreva, E.; Traina, P.; Marcantoni, A.; Picollo, F.; **Kvaková, K.**; Cígler, P.; Degiovanni, I. P.; Carabelli, V.; Genovese, M

Temperature is a vital physical parameter that significantly influences many biological processes. Moreover, alternations in intracellular temperature often reflect pathological changes. Despite these implications, our ability to monitor temperature at the intracellular level is limited.

In this study, we utilized a single-photon-sensitive confocal microscope equipped for ODMR (Viz. Chapter 1.5.3) measurements to study the effects of neuronal activity on intracellular temperature variations (Figure 9A). For temperature sensing, FNDs were incubated with hippocampal neurons for 5h at 0.6 μg/ml (Figure 9C). The temperature measurements were conducted under three different conditions: 1. natural firing activity (CTRL), 2. enhanced firing activity after the addition of a GABA inhibitor (picrotoxin), and 3. inhibition of spontaneous firing with tetrodotoxin (TTX) and cadmium chloride (Cd) (Figure 9B). The first experimental conditions revealed no significant temperature variations; therefore, we could exclude possible thermal exchanges related to the perfusion system. Following the preliminary experiment, in the subsequent phase, we wanted to determine if neuronal activity alterations are associated with temperature fluctuations. The second condition led to a noticeable temperature increase linked to the heightened firing rate. When the network activity was silenced, a substantial temperature decrease was observed in the third condition. The temperature variations (1°C) associated with neuronal firing potentiation and inhibition are shown in (Figure 9D).

In addition, an examination was conducted to ascertain whether the exposure to the laser, microwave radiation, and the incubation process with FNDs could potentially influence the inherent activity of the hippocampal neurons during the implementation of the ODMR measurement procedure. Laser exposure, microwave radiation, and incubation with FNDs (≈200 nm) did not affect spontaneous firing activity, confirming cell excitability and ion channel functionality which agreed with the previous findings (Guarina et al., 2018).

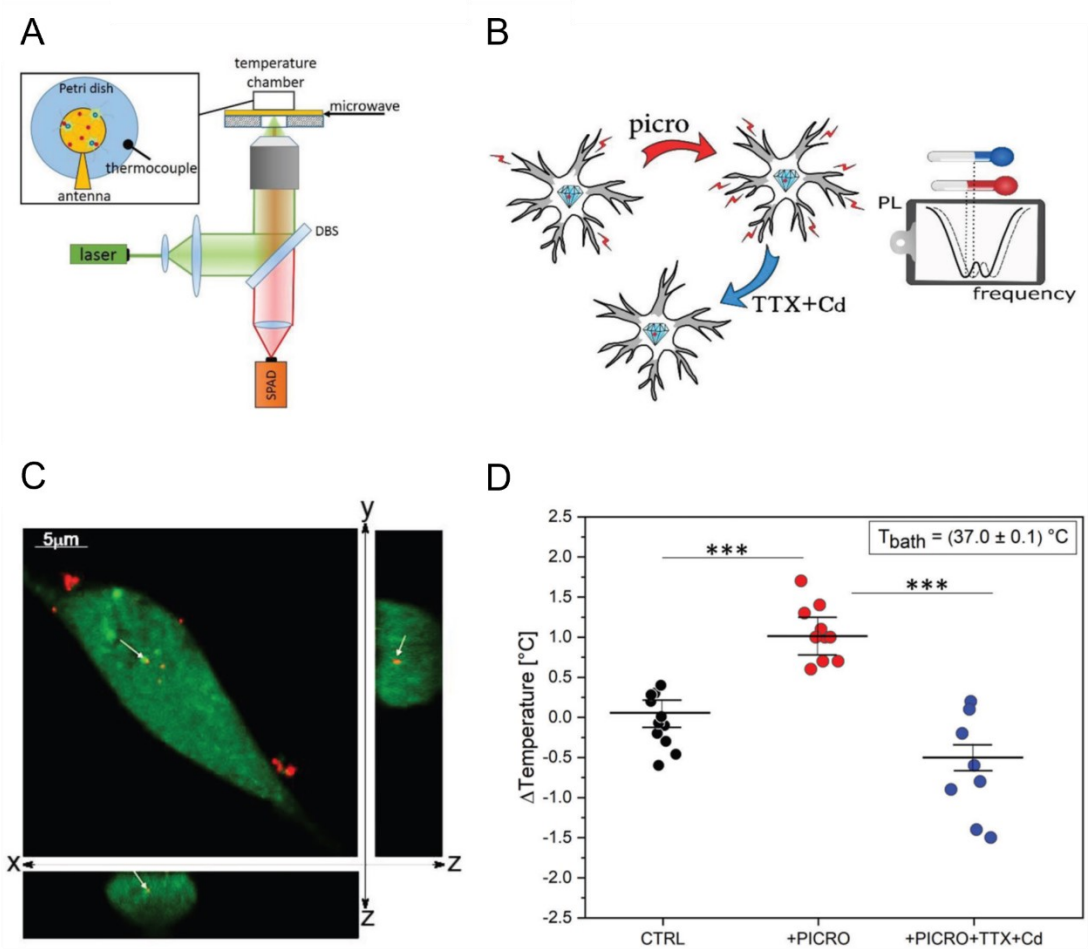

Figure 9: General scheme of the study A) Scheme of ODMR measurement setup. B) Scheme of the experimental conditions for the measurement. C) Confocal fluorescence micrograph of hippocampal neurons incubated with FNDs (0.6 µg/ml) for 5h. Green color – cytoplasm staining, red color - FND emission. White arrows show internalized single FNDs D) Boxplot of temperature variations measured at different conditions.

The obtained results support the conclusion that the observed alternation in temperature during the experiment is directly correlated with the modified firing activity of hippocampal neurons. Coupled with the high sensitivity of this technique, FNDs provide a route toward the comprehensive investigation of localized temperature fluctuations under physiological and pathological conditions.

My contribution:

I prepared (air oxidation, wet oxidation, annealing) and characterized fluorescence nanodiamond samples (DLS, spectroscopy). I contributed to the manuscript preparation.

4.3 Synthesis of Near-Infrared Emitting Gold Nanoclusters for Biological Applications.

Pramanik, G.; Keprova, A.; Valenta, J.; Bocan, V.; **Kvaková, K.**; Libusova, L.; Cigler, P.

NIR-emitting AuNCs exhibit significant potential as long-term imaging tools for both *in vitro* and *in vivo* applications.; however, their biggest drawback is their quantum yield which is very low. This work demonstrates a facile bottom-up approach to prepare water-soluble NIR-emitting PL AuNCs with enhanced quantum yield. In this synthesis process, ultrasmall AuNCs were prepared from a solution of gold precursor ($HAuCl_4$), which was treated with thioctic acid and thiol-terminated PEG (Mw 2,000), leading to the reduction of Au^{3+} ions resulting in ultrasmall AuNCs (Figure 10, **1**). The synthetic conditions were carefully adjusted to avoid the formation of large NPs due to the potential aggregation of metal ions during a reduction in aqueous solutions (Shang et al., 2011). The surface of AuNCs significantly impacts the stability, as well as the electronic and optical characteristics of these particles (Wu and Jin, 2010). Hence, selecting appropriate ligands stabilizing ultrasmall clusters is crucial for preparing highly photoluminescent AuNCs. Ligands containing thiol groups are frequently employed for synthesizing AuNCs due to the robust covalent bonds between thiols and gold. Previous investigation suggests that ligands containing multiple thiol groups outperform those with a single thiol group in stabilizing photoluminescent AuNCs (Oh et al., 2010), which is attributed to the greater number of binding sites that multi-thiol ligands provide, leading to enhanced colloidal stability of AuNCs. Therefore, thioctic acid (bidentate thiol) was used for the AuNC stabilization. In addition to enabling precise size control during the growth of NPs in an aqueous environment, thioctic acid plays a crucial role in introducing a carboxylic acid group on the surface of the NPs. The new functionality enables further conjugation of compounds with biological relevance (Nair et al., 2015; Porret et al., 2017). However, thioctic acid-stabilized AuNCs showed poor colloidal stability, especially at acidic pH, due to the protonation of carboxylate groups, limiting stabilization caused by the electrostatic repulsion. Therefore, thioctic acid-AuNCs were subsequently modified by thiol-terminated PEG to provide electrosteric stabilization. This modification gives us particles with increased colloidal stability even in high-ionic strength environments and at different pH, making them suitable

candidates for applications in biological systems. Carboxylic acid groups on the surface of AuNCs (**1**) can be linked to amines *via* amide bonds using carbodiimide-based coupling reagents (Bartczak and Kanaras, 2011). Therefore, the AuNCs (**1**) were further functionalized with TPP bromide using 1-ethyl-3-(dimethylaminopropyl) carbodiimide hydrochloride (EDC) reagent (Figure 10, **2**).

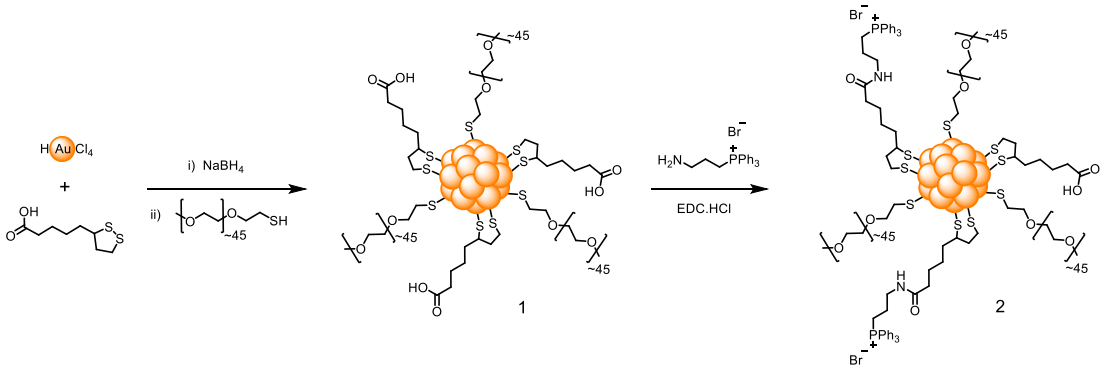

*Figure 10: Preparation of NIR-emitting photoluminescent AuNCs - synthesis leading to thioctic acid-PEG-stabilized AuNCs (**1**) and further modification to obtain triphenylphosphonium-containing AuNCs (**2**).*

As expected, the absorption spectra of AuNCs (**1, 2**) indicated lack of surface plasmon band (Figure 11A) but showed broad emission from 550 nm to 850 nm (Figure 11B). However, TPP-functionalized AuNCs (**2**) displayed enhanced PL. Since colloidal stability and core size, analyzed by high-resolution scanning transmission electron microscopy (HR-STEM), did not change after the amidic coupling. Therefore, the PL enhancement occurred as a result of the metal-to-ligand charge transfer (Pramanik et al., 2018).

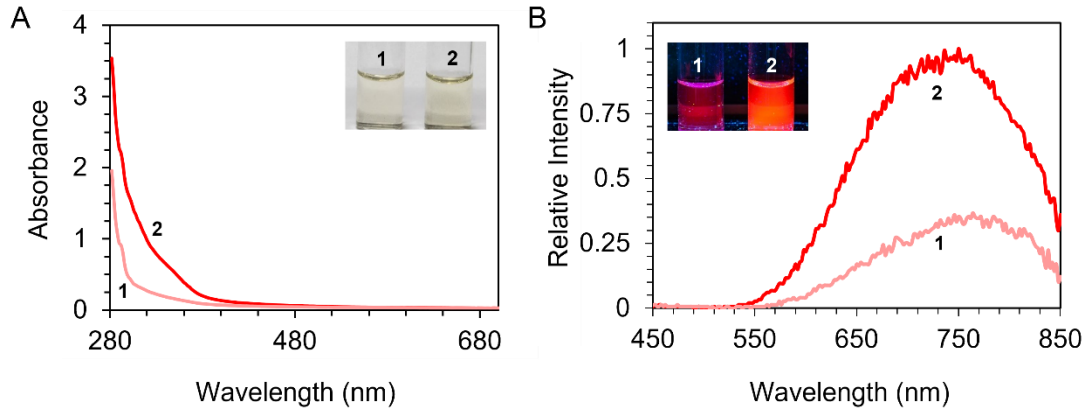

*Figure 11: A) Absorption spectra showing no plasmon peak for both AuNCs (**1**) and (**2**), inset - photograph of AuNC (**1**) and (**2**) solutions in water under white light. B) Photoluminescent spectra showing increased PL after amidic coupling, inset - photograph of the AuNC (**1**) and (**2**) solutions in water under UV light (365 nm).*

The potential cytotoxicity of the AuNCs (**2**) was tested on HeLa cells, showing no loss of cell viability compared to control cells, thus suggesting the biocompatibility of AuNCs (**2**) and their potential as fluorescent probes for bioimaging applications. The AuNCs (**1**, **2**) exhibited a broad emission of around ~750 nm when excited with a 405 nm laser, allowing for reliable distinction from the exciting light source. The TPP-modified AuNCs (**2**) were tested on HeLa cells and monitored using a flow cytometer. The HeLa cells were incubated with varying concentrations of TPP-modified AuNCs (**2**) (0.5 mg/mL to 2 mg/mL) for 2 hours, and the NIR PL (>720 nm) was observed to be dependent on both the incubation time and the concentration of the AuNCs (**2**). The maximal fluorescence intensity was observed with the 780/60 bandpass filter (data shown in publication, Fig 3).

Finally, non-invasive imaging of AuNCs within the cells was conducted using a standard confocal laser scanning microscope (CLSM). After 24 hours of incubation with TPP-containing AuNCs, bright red PL was observed inside the HeLa cells (Figure 12), indicating successful cellular uptake of the NPs. Our findings suggest that the highly colloidally stable, biocompatible AuNCs with bright NIR PL have promising potential for biomedical applications, particularly in cellular imaging.

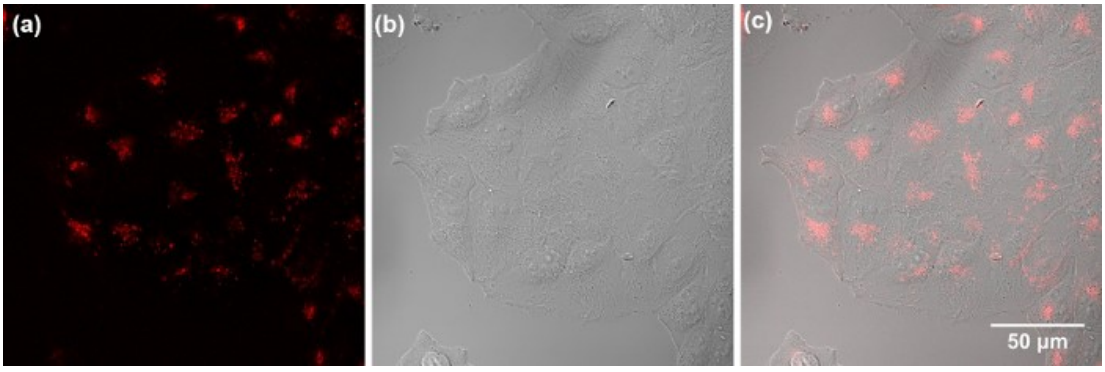

*Figure 12: HeLa labeled with prepared TPP containing AuNCs (**2**) – CLSM imaging. HeLa cells were incubated with 200 µg/ml of the AuNCs (**2**) for 24h. A) Denotes the red fluorescence channel B) transmitted channel (DIC). C) Overlay A) and B).*

My contribution:

I synthesized and characterized gold nanoclusters. I contributed to the manuscript preparation and design of the biological experiments.

4.4 Inverse Heavy-Atom Effect in Near Infrared Photoluminescent Gold Nanoclusters.

Pramanik, G.; **Kvakova, K.**; Thottappali, M. A.; Rais, D.; Pfleger, J.; Greben, M.; El-Zoka, A.; Bals, S.; Dracinsky, M.; Valenta, J.; Cigler, P.

Driven by our curiosity regarding the influence of surface capping ligands on the optical properties of AuNCs, we investigated the effect of heavy atoms within the ligand sphere on the optical characteristics of AuNCs. This study presents the effect of an iodine-functionalized ligand on the optical features of NIR PL AuNCs and reveals a phenomenon in contrast with the heavy atom effect described so far.

In this work, we also employed a previously published synthetic approach for preparation NIR emitting AuNCs stabilized by the effect of multidentate thioctic acid and thiol-containing PEG moieties resulting in thioctic and PEG-protected AuNCs (Pramanik et al., 2020) (Figure 13, **1**). To examine the impact of a heavy atom within the ligand sphere on AuNC optical properties, 4-iodobenzylamine was coupled with carboxylic groups present on the thioctic acid- and PEG-protected AuNC surface employing EDC coupling to form iodine-containing AuNCs (Figure 13, **4**). This iodine-containing ligand was chosen for its stability and reactivity. The control compound was prepared by coupling TA and PEG-protected AuNCs with benzylamine (Figure 13, **3**).

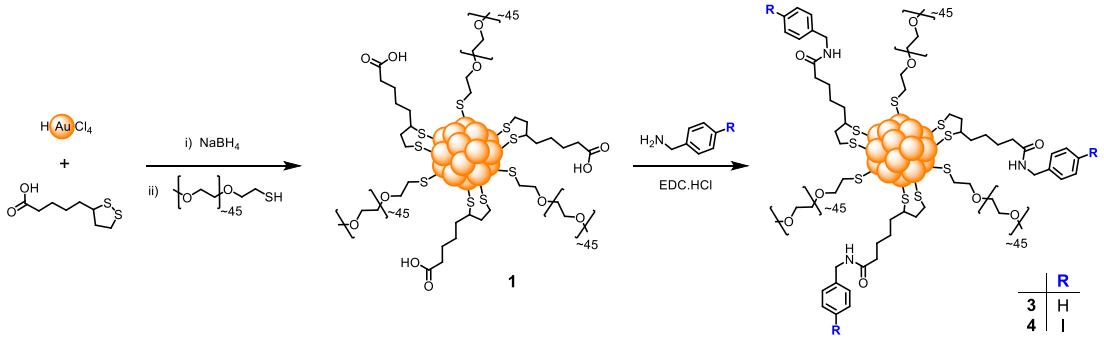

*Figure 13: Synthesis of benzylamine-modified AuNCs (control sample, **3**) and iodine-containing AuNCs (**4**) using previously described thioctic acid- PEG-AuNCs as intermediate (**1**).*

Inductively coupled plasma-optical emission spectroscopy (ICP-OES) and elemental analysis were used to obtain the ratio of Au and the attached ligand of AuNCs. The results showed Au/S and Au/N molar ratios that were comparable for both iodine-containing AuNCs (**4**) and control AuNCs (**3**), indicating identical ligand stoichiometry and substitution levels. The successful modification by benzyl

moiety was confirmed by ^{1}H NMR spectroscopy. The elemental composition of small molecule functionalized AuNCs was previously analyzed using electrospray ionisation - mass spectrometry (ESI-MS) (Chen et al., 2019; Yu et al., 2014; Yuan et al., 2014). However, our attempt to determine the elemental composition using ESI-MS was inconclusive, presumably due to high molecular weight ligands (PEG) attenuating the overall ionization.

These ultrasmall AuNCs (**1, 3, 4**) also lack the characteristic surface plasmon resonance absorption around 520 nm (Figure 14A). Their PL was observed in the visible-to-NIR region, with the maximum at approximately 740 nm (Figure ***14***B), suggesting about 25-32 atoms per cluster. The PL intensity increased when benzylamine was added, suggesting the benzyl group's electron-donating ability (Wu and Jin, 2010). Despite similar conjugation, iodine-containing AuNC (**4**) showed slightly higher PL intensity than AuNCs (**3**) without iodine.

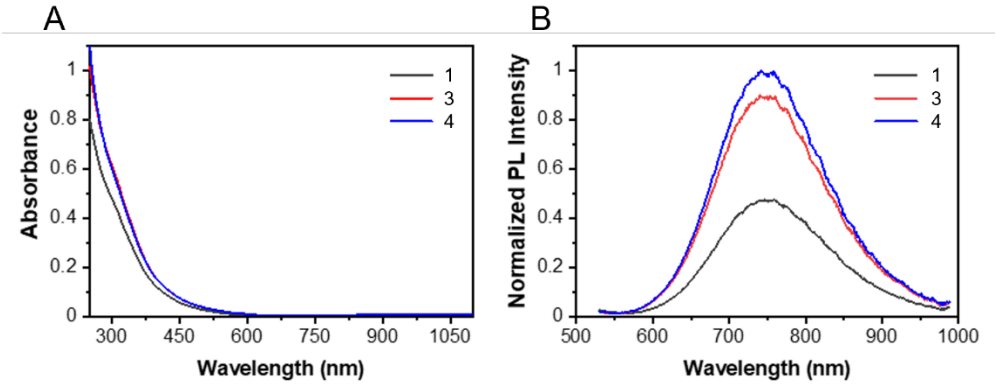

*Figure 14: A) Absorption spectra of prepared AuNCs in water (**1, 3, 4**) – all without plasmon band. B) Emission spectra of AuNC (**1, 3, 4**) in water – iodine-modified AuNCs (**4**) showed slightly higher emission than the control sample (**3**). Reproduced and adapted from the literature (Pramanik et al., 2021)*

The PL quantum yields were about 11 % and 15 %, respectively (results shown in the publication, Figure S3). Compared to the control sample AuNCs (**3**) (1.64 μs), the longer PL decay in iodine-containing AuNCs (**4**) (1.75 μs) can likely be attributed to iodine's electron-rich nature facilitating enhanced radiative decay from the triplet excited state. This finding of longer PL lifetime and higher quantum yield upon adding heavy atom iodine contradicts the typical behavior of fluorophores upon heavy atom addition, known as the heavy atom effect (Lakowicz, 2009). Given that the HR-STEM results demonstrate a similar size of iodine-containing AuNCs (**4**) and control (**3**), thus no significant aggregation occurred, and we can exclude the

possibility of previously described aggregation-induced anti-HAE (Xu et al., 2019). These findings of the inverse heavy atom effect may lead to further investigation of iodine and other heavy elements for tuning the exciton lifetime ultrasmall metal nanoclusters PL. A prolonged PL lifetime can be beneficial for AuNC's applications in bioimaging.

My contribution:

I synthesized and characterized gold nanoclusters. I contributed to the manuscript preparation.

4.5 Reversible Photo- and Thermal-Effects on the Luminescence of Gold Nanoclusters: Implications for Nanothermometry.

Valenta, J.; Greben, M.; Pramanik, G.; **Kvakova, K.**; Cigler, P.

While the knowledge surrounding AuNCs continues to grow, there is still a lack of comprehensive investigations into their photophysical properties, particularly regarding the relationship between PL and factors such as excitation power and solution temperature. This study presents an investigation that uncovers transient and completely reversible alterations in PL amplitude and decay kinetics attributable to heating induced by power dissipation.

A previously published procedure (Pramanik et al., 2020) was used to synthesize benzylamine containing TA- and PEG-stabilized AuNCs (**3**). After the synthesis, the absorption spectra of AuNC (**3**) water solutions were measured. As expected, the absorption spectra did not reveal the plasmon bands, characteristic of bigger AuNPs, but it also did not show any other specific bands. Therefore, the 2nd derivative was calculated to find influential bands (Figure 14A). The bands at photon energy higher than 2 eV align well with a previously described theoretical model of thiolated $Au_{25}(SH)_{18}$ clusters (Zhu et al., 2008). At photon energy lower than 2 eV, a weak absorption tail overlapping with the onset of the PL band was observed. This is similar to transitions observed at low temperatures in Au_{20} clusters in a Ne matrix (Yu et al., 2017). These findings underscore the Au core's role in this spectral range's absorption. Furthermore, the photoluminescence excitation (PLE) spectra depict similar features to the absorbance spectra. The spectral dependence of the PL external quantum yield (EQY) stays around 10 %, mostly unaffected by the excitation wavelength, with a modest peak of 14 % at 2.2 eV (Figure 14B).

During the investigation, slow transient PL quenching of AuNCs (**3**) was revealed. The potential cause could be AuNCs (**3**) heating due to dissipated laser power. We measured the PL spectra and decay kinetics for a sample in a heated/cooled holder to test this. The excitation power was below saturation, and the temperature varied between 5 and 85 °C. PL intensity decreased by about 70 % when increasing the temperature from 20 to 85 °C. However, a greater decrease was induced by excitation power, implying intense heating to temperatures around 100 °C

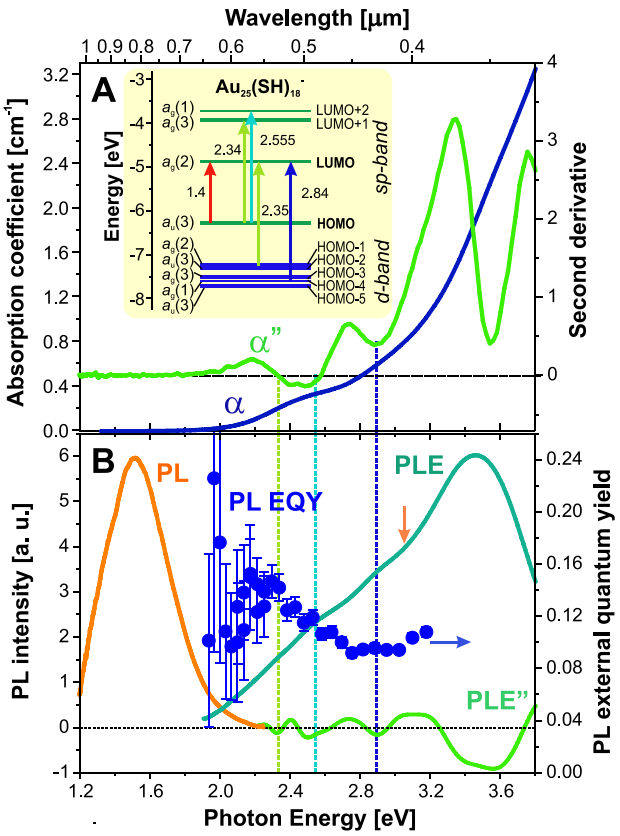

Figure 15: A) Blue line – absorption coefficient, green line 2nd derivative of the absorption coefficient. B) Orange line and arrow – PL excited at 410 nm, blue-green line – PL excitation detected at 740 nm, green line – 2nd derivative of the PL excitation and blue dots – quantum yields

(although this is a false value influenced by blinking and especially the dark state of AuNCs (**3**)). On the other hand, the excitation power caused relatively small (~20 % reduction) AuNC (**3**) excited state lifetime shortening compared to the significant effect of heating, which reduced the lifetime to less than half (data shown in the publication, Figure 6).

Additionally, PL blinking of AuNCs (**3**) was observed under continuous 405 nm excitation above the saturation level. In the measurement setup, we measured a droplet of diluted solution on a silica cover glass which ensured that only AuNCs (**3**) adsorbed on the silica surface were in focus, providing localized signals. Although, the particles were measured after evaporation, and thus the results do not help us understand AuNCs (**3**) behavior in solutions. Due to the long PL decay time of the studied AuNCs (**3**), longer detection times were required to achieve good signal-to-noise ratios. An example of a PL time trace (600 s) from one emitting spot revealed three bright periods with a bright-to-dark state ratio of about 1:4 (Figure 16).

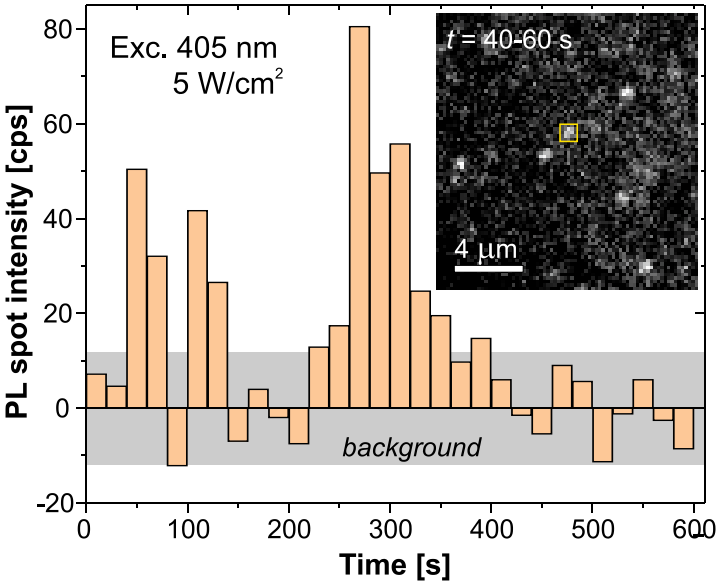

Figure 16: Single AuNC integrated PL signal time-trace (obtained from the sequence of photoluminescent images (30x20 s). The inset picture shows part of the 3rd image with a featured dot indicated by the yellow square. The variation in the background signal is marked by grey.

AuNCs' temperature-dependent PL decay time was already utilized for nano thermometry (Shang et al., 2013), achieving approximately 1 % change per 1 °C. Despite our data exhibiting non-linearity, a similar percentage change was observed after linear fitting between 20 and 45 °C. In previous research (Shang et al., 2013), time-correlated single photon counting (short-pulse limit) was used, but we applied the long-pulse limit. Moreover, our approach extends thermometry up to 90 °C, with a slight decrease in sensitivity. However, excitation power should be kept below the PL saturation limit to prevent local temperature rise due to laser power dissipation. This thermo-sensitivity seems universal in AuNCs, but different clusters (size, modifications with ligands) need their calibration for thermometry. Moreover, AuNC prepared by us demonstrated high stability through saturation and heating cycles with no permanent changes in PL characteristics. The observed reversible changes in luminescence dependent on light exposure and temperature may broaden AuNCs applications in bio-imaging, thermometry, and sensing.

My contribution:

I synthesized and characterized gold nanoclusters. I contributed to the manuscript preparation.

4.6 Optically Coupled Gold Nanostructures: Plasmon Enhanced Luminescence from Gold Nanorodnanocluster Hybrids

Pavelka, O.; **Kvakova, K.**; Vesely, J.; Mizera, J.; Cigler, P.; Valenta, J.

In this work, we show a simple synthetic protocol for the fabrication of hybrid AuNR@AuNC particles (Figure 17), with the ability to tune AuNCs luminescence by plasmonic enhancement in order to extend the AuNC applications in the biomedical field. Plasmonic enhancement is frequently used to improve weak fluorophore performance; however, poorly described for AuNC yet.

AuNRs were prepared by a slightly modified seeded growth procedure (Nikoobakht and El-Sayed, 2003) after a homogenous silica shell (thicknesses 5 nm and 12nm) was grown employing the previously described method (Pavelka et al., 2021), resulting in Au@SiO_2 NRs. The silica layer in this system serves as a transparent spacer with adjustable thickness separating AuNCs (Pramanik et al., 2020) from AuNRs because the separation distance between plasmonic and luminescent parts is critical as enhancement or quenching processes are distance-dependent (Chen et al., 2013; Mertens et al., 2007). In general, a thin shell allows for higher excitation of AuNCs by the AuNRs; nevertheless, at close distances, a substantial energy transfer from fluorophore to metal can occur, reducing luminescence efficiency dramatically. For several NIR-emitting fluorophores, an optimum distance of about 10-12 nm was previously described (Qin et al., 2018a). Ultrasmall, positively charged TPP-modified AuNCs (**2**) were subsequently attached to negatively charged Au@SiO_2 NRs surface (Pavelka et al., 2021) *via* coulombic attraction. The resulting particles were analyzed by electron microscopy.

Unbound TPP-modified AuNCs (**2**) were washed out to not affect further measurements. Moreover, we were interested in binding stoichiometry, which is essential in this study, even though rarely discussed, even in cases where PL enhancement is described (Kim and Jang, 2017; Qin et al., 2018b). The stoichiometry calculations sometimes claim 10^4-10^5 AuNCs per single plasmonic NPs (Kim and Jang, 2017); other works show approx. 40 AuNCs per AuNR (Qin et al., 2015). As long as NCs and NRs are both made of gold, ICP-OES cannot be employed to quantify the AuNC amount per AuNR. Therefore, stoichiometry was determined using neutron activation of AuNCs (**2**) to obtain mildly radioactive 198Au and quantify the number of AuNCs (**2**) on the Au@SiO_2NR by measuring radioactivity.

The calculated amount of AuNCs (**2**) per single AuNR was 930 (silica shell thickness 5 nm) and 1290 (silica shell thickness 12 nm); both cases correspond to the surface coverage ≈ of 20 %; thus, AuNC amount is not shell thickness dependent.

After knowing the stoichiometry of Au@SiO_2NR, PL intensity excitation enhancement was investigated at excitation at 510 and 630 nm. These wavelengths were chosen because they match the plasmonic bands of AuNRs. The PL enhancement 4.4-fold was measured for the Au@SiO_2NR sample with a 5 nm silica layer excited at 633 nm and 3.2 (20 % of maximum load AuNCs (**2**) per AuNR). In the case of a 12 nm thick silica shell and excitation 633 nm, the enhancement was 3.2-fold. The enhancement at 510 nm is minimal for both Au@SiO_2 NRs and barely compensates for absorption. Therefore, excitation wavelength matching longitudinal plasmon and smaller distance between AuNCs (**2**) and AuNRs provided the highest enhancement. The improved PL emission of the Au@SiO_2NRs should make fluorescence detection and tracking easier, even at a single particle level. This finding, coupled with red/NIR emission, makes prepared Au@SiO_2NRs attractive for bioimaging.

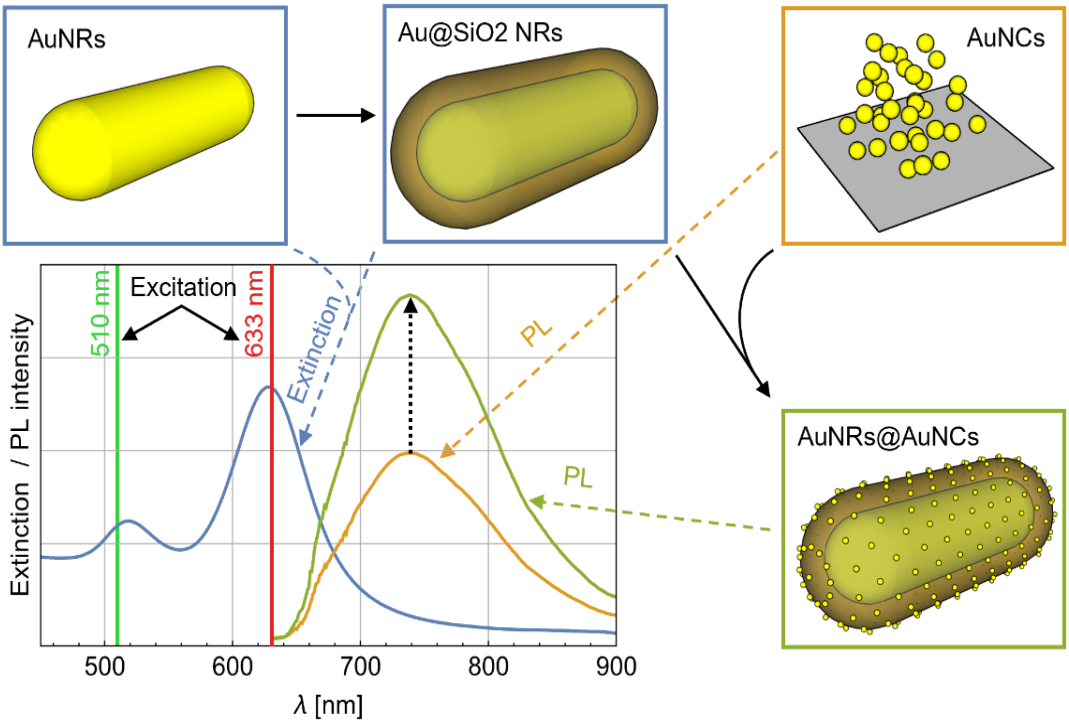

*Figure 17: General scheme of the study. The localized surface plasmon resonance (LSPR) bands of AuNRs (510 and 633 nm) offset from the PL emission band of AuNCs (**2**). AuNC (**2**) PL enhancement after attaching AuNCs onto AuNRs (black arrow).*

My contribution:

I synthesized and characterized gold nanoclusters and prepared complexes of gold nanoclusters with gold nanorods. I contributed to their characterization and to the manuscript preparation.

4.7 Towards Site-specific Emission Enhancement of Gold Nanoclusters Using Plasmonic Systems: Advantages and Limitations

Pavelka, O.; Dyakov, S. A.; **Kvakova, K**.; Vesely, J.; Cigler, P.; Valenta, J.

This work presents extensive spectroscopic examination and analysis of AuNC (**2**) PL enhancement after combining them with plasmonic AuNRs (Figure 18). The same AuNP combination previously described (Pavelka et al., 2022) was used to investigate emission enhancement (≈10^3 AuNCs (**2**) per single nanorod). The main benefits of our AuNC@AuNR system are geometrical flexibility, optical tunability, and a unique level of structure control.

Besides previously described results (distance-dependent AuNC (**2**) PL enhancement), we discovered that precise localization of AuNCs on the AuNRs surface also strongly impacts the AuNC (**2**) PL. This was revealed by analysis of the PL spectra of AuNRs@AuNCs, where we could differentiate the coupled and non-coupled components (data shown in the publication, Fig 4).

In addition to the spectroscopic characterization, we performed boundary element method (García De Abajo and Howie, 2002) calculations that perfectly matched the experimental results. The calculations enabled us to identify the potential of enhancing PL by increasing the volume of AuNRs.

Based on calculations, we also found that theoretical maximum emission enhancement is lower than excitation enhancement and does not improve the utilization of AuNCs as luminescent particles. Increasing the enhancement factor could be achieved by avoiding non-coupled particles on AuNRs' side by growing a silica shell solely on nanorod tips. Such a synthetic method was demonstrated by Meyer and Murphy (2022). Lastly, our methodological approach can be beneficial for analogous studies of plasmonic systems involving AuNRs for a suitable fluorophore emission enhancement.

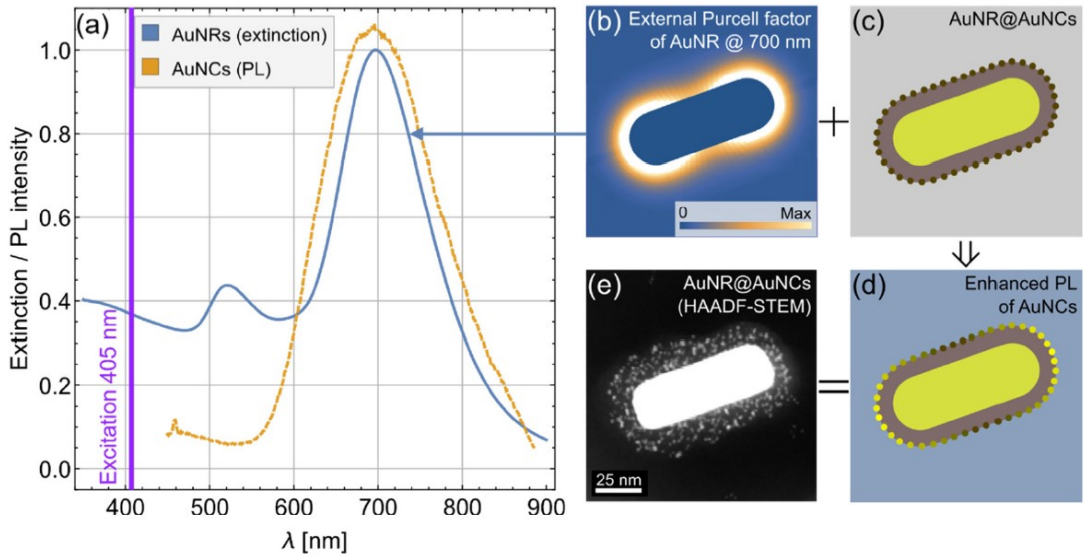

*Figure 18: Scheme of AuNC (**2**) PL emission of AuNCs (**2**) boosted after attachment to AuNRs. A) The longitudinal localized surface plasmon resonance (LSPR) band of AuNRs and the PL band of AuNCs (**2**) overlap at 700 nm, whereas the excitation wavelength (405 nm) does not align with any LSPR bands of the AuNRs. (b) The map displays the external Purcell factor surrounding a single AuNR. (c) The assumption of a homogenous coverage of AuNCs (**2**) over an Au@SiO2 NR is corroborated by (e) HAADF-STEM imaging.*

My contribution:

I synthesized and characterized gold nanoclusters and also prepared complexes of gold nanoclusters with gold nanorods. I contributed to their characterization and to the manuscript preparation.

5 CONCLUSIONS

In conclusion, this thesis has presented an in-depth investigation into the potential of FNDs and AuNCs as promising NIR emitting fluorescent probes for biomedical applications. The study thoroughly explored their synthesis, modifications, properties, and possible applications of these NPs. Our study successfully answered all our hypotheses listed within the aims.

First, ultrabright FNDs with narrow size distribution (≈200 nm) were successfully isolated and bio-compatibilized by a structurally dense layer of alkyne-terminated polyglycerol. The alkyne functionalization enabled a covalent attachment of mannose using a bioconjugation technique. *In vitro* evaluation showed increased mannosylated FNDs uptake by macrophages and enhanced retention in mice sentinel LNs compared to non-mannosylated FNDs. The 200 nm FNDs were also investigated as ODMR temperature sensors, and it was shown that they provide a tool for high-sensitivity temperature measurement at a single cell level. It was possible to monitor temperature variations during hippocampal neuron firing alternations. These findings open new avenues for localized-temperature measurements at physiological and pathological conditions with high sensitivity.

Furthermore, we have successfully devised a technique to synthesize NIR emitting AuNCs utilizing thioctic acid and PEG for stabilization. This innovative synthesis approach has not only provided colloidally stable particles but has also allowed for the improvement of the quantum yield of the AuNCs through the attachment of TPP. To our surprise, the addition of a heavy atom in the form of iodine resulted in an extension of the fluorescence lifetime of the AuNCs. Moreover, prepared AuNCs did not show cell viability loss, suggesting their non-cytotoxicity and biocompatibility. AuNCs were internalized by HeLa cells and visualized using confocal laser scanning microscopy. These observations underline the potential utility of AuNCs in cellular imaging and other biomedical applications. Besides ligands, AuNRs were investigated as potential enhancers of AuNC PL owing to their tunable plasmonic properties. We demonstrated an easy method to prepare AuNRs@AuNCs particles with a silica layer as a spacer with tunable thickness. The use of these nanoantennas resulted in a boost of AuNC PL, facilitating their detection and tracking *via* fluorescence microscopy, even at the

single-particle level. Consequently, the AuNC @ AuNR system emerges as a potential tool for applications in bioimaging.

In summary, our research supports the claim that FNDs and AuNCs are promising candidates for NIR-emitting fluorescent probes in biomedical applications. However, further investigation and thorough understanding are still required to achieve their full potential.

6 LIST OF PUBLICATIONS

All findings obtained during my Ph.D. study have been compiled into seven scientific publications, published in peer-reviewed journals, where I contributed as a first author or co-author.

Publications *in extenso* that constitutes the basis of the Ph.D. thesis:

(Listed in reverse chronological order.)

1. Pavelka, O.; Dyakov, S. A.; **Kvakova, K**.; Vesely, J.; Cigler, P.; Valenta, J. Towards Site-Specific Emission Enhancement of Gold Nanoclusters Using Plasmonic Systems: Advantages and Limitations. *Nanoscale* 2023. **IF=8.3; Q1**
2. Petrini, G.; Tomagra, G.; Bernardi, E.; Moreva, E.; Traina, P.; Marcantoni, A.; Picollo, F.; **Kvaková, K.**; Cígler, P.; Degiovanni, I. P.; Carabelli, V.; Genovese, M. Nanodiamond–Quantum Sensors Reveal Temperature Variation Associated to Hippocampal Neurons Firing. *Adv. Sci.* 2022. **IF=17.5; Q1**
3. **Kvakova, K.**; Ondra, M.; Schimer, J.; Petrik, M.; Novy, Z.; Raabova, H.; Hajduch, M.; Cigler, P. Visualization of Sentinel Lymph Nodes with Mannosylated Fluorescent Nanodiamonds. *Adv Funct Materials* 2022. **IF=19.9; Q1**
4. Pavelka, O.; **Kvakova, K.**; Vesely, J.; Mizera, J.; Cigler, P.; Valenta, J. Optically Coupled Gold Nanostructures: Plasmon Enhanced Luminescence from Gold Nanorod-Nanocluster Hybrids. *Nanoscale* 2022. **IF=8.3; Q1**
5. Pramanik, G.; **Kvakova, K.**; Thottappali, M. A.; Rais, D.; Pfleger, J.; Greben, M.; El-Zoka, A.; Bals, S.; Dracinsky, M.; Valenta, J.; Cigler, P. Inverse Heavy-Atom Effect in near Infrared Photoluminescent Gold Nanoclusters. *Nanoscale* 2021. **IF=8.3; Q1**
6. Valenta, J.; Greben, M.; Pramanik, G.; **Kvakova, K.**; Cigler, P. Reversible Photo- and Thermal-Effects on the Luminescence of Gold Nanoclusters: Implications for Nanothermometry. *Phys. Chem. Chem. Phys.* 2021. **IF=3.9; Q2**
7. Pramanik, G.; Keprova, A.; Valenta, J.; Bocan, V.; **Kvaková, K.**; Libusova, L.; Cigler, P. Synthesis of Near-Infrared Emitting Gold Nanoclusters for Biological Applications. *JoVE* 2020. **IF=1.4; Q3**

7 REFERENCES

Acerbi, F., Broggi, M., Eoli, M., Anghileri, E., Cuppini, L., Pollo, B., Schiariti, M., Visintini, S., Orsi, C., Franzini, A., Broggi, G., Ferroli, P., 2013. Fluorescein-guided surgery for grade IV gliomas with a dedicated filter on the surgical microscope: preliminary results in 12 cases. Acta Neurochir 155, 1277–1286. https://doi.org/10.1007/s00701-013-1734-9

Ahmed, M., Purushotham, A.D., Douek, M., 2014. Novel techniques for sentinel lymph node biopsy in breast cancer: a systematic review. The Lancet Oncology 15, e351–e362. https://doi.org/10.1016/S1470-2045(13)70590-4

Albanese, A., Chan, W.C.W., 2011. Effect of Gold Nanoparticle Aggregation on Cell Uptake and Toxicity. ACS Nano 5, 5478–5489. https://doi.org/10.1021/nn2007496

Alford, R., Simpson, H.M., Duberman, J., Hill, G.C., Ogawa, M., Regino, C., Kobayashi, H., Choyke, P.L., 2009. Toxicity of organic fluorophores used in molecular imaging: literature review. Mol Imaging 8, 341–354.

Alhaddad, A., Adam, M.-P., Botsoa, J., Dantelle, G., Perruchas, S., Gacoin, T., Mansuy, C., Lavielle, S., Malvy, C., Treussart, F., Bertrand, J.-R., 2011. Nanodiamond as a Vector for siRNA Delivery to Ewing Sarcoma Cells. Small 7, 3087–3095. https://doi.org/10.1002/smll.201101193

Amoozgar, Z., Yeo, Y., 2012. Recent advances in stealth coating of nanoparticle drug delivery systems. Wiley Interdisciplinary Reviews: Nanomedicine and Nanobiotechnology 4, 219–233. https://doi.org/10.1002/wnan.1157

Ang, C.H., Tan, M.Y., Teo, C., Seah, D.W., Chen, J.C., Chan, M.Y.P., Tan, E.Y., 2014. Blue dye is sufficient for sentinel lymph node biopsy in breast cancer. British Journal of Surgery 101, 383–389. https://doi.org/10.1002/bjs.9390

Ankersmit, M., Bonjer, H.J., Hannink, G., Schoonmade, L.J., Van Der Pas, M.H.G.M., Meijerink, W.J.H.J., 2019. Near-infrared fluorescence imaging for sentinel lymph node identification in colon cancer: a prospective single-center study and systematic review with meta-analysis. Tech Coloproctol 23, 1113–1126. https://doi.org/10.1007/s10151-019-02107-6

Barone, F.C., Marcinkiewicz, C., Li, J., Sternberg, M., Lelkes, P.I., Dikin, D.A., Bergold, P.J., Gerstenhaber, J.A., Feuerstein, G., 2018. Pilot study on biocompatibility of fluorescent nanodiamond-(NV)-Z~800 particles in rats: safety, pharmacokinetics, and bio-distribution (part III). IJN Volume 13, 5449–5468. https://doi.org/10.2147/IJN.S171117

Bartczak, D., Kanaras, A.G., 2011. Preparation of Peptide-Functionalized Gold Nanoparticles Using One Pot EDC/Sulfo-NHS Coupling. Langmuir 27, 10119–10123. https://doi.org/10.1021/la2022177

Barton, J., Gulka, M., Tarabek, J., Mindarava, Y., Wang, Z., Schimer, J., Raabova, H., Bednar, J., Plenio, M.B., Jelezko, F., Nesladek, M., Cigler, P., 2020. Nanoscale Dynamic Readout of a Chemical Redox Process Using Radicals Coupled with Nitrogen-Vacancy Centers in Nanodiamonds. ACS Nano 14, 12938–12950. https://doi.org/10.1021/acsnano.0c04010

Becker, W., 2012. Fluorescence lifetime imaging - techniques and applications: FLUORESCENCE LIFETIME IMAGING. Journal of Microscopy 247, 119–136. https://doi.org/10.1111/j.1365-2818.2012.03618.x

Berezin, M.Y., Achilefu, S., 2010. Fluorescence Lifetime Measurements and Biological Imaging. Chem. Rev. 110, 2641–2684. https://doi.org/10.1021/cr900343z

Berezin, M.Y., Guo, K., Akers, W., Livingston, J., Solomon, M., Lee, H., Liang, K., Agee, A., Achilefu, S., 2011. Rational Approach To Select Small Peptide Molecular Probes Labeled with Fluorescent Cyanine Dyes for in Vivo Optical Imaging. Biochemistry 50, 2691–2700. https://doi.org/10.1021/bi2000966

Blanco, E., Shen, H., Ferrari, M., 2015. Principles of nanoparticle design for overcoming biological barriers to drug delivery. Nature Biotechnology 33, 941–951. https://doi.org/10.1038/nbt.3330

Bolaños, K., Kogan, M.J., Araya, E., 2019. Capping gold nanoparticles with albumin to improve their biomedical properties. IJN Volume 14, 6387–6406. https://doi.org/10.2147/IJN.S210992

Broadwater, D., Bates, M., Jayaram, M., Young, M., He, J., Raithel, A.L., Hamann, T.W., Zhang, W., Borhan, B., Lunt, R.R., Lunt, S.Y., 2019. Modulating cellular cytotoxicity and phototoxicity of fluorescent organic salts through counterion pairing. Sci Rep 9, 15288. https://doi.org/10.1038/s41598-019-51593-z

Caracciolo, G., 2018. Clinically approved liposomal nanomedicines: lessons learned from the biomolecular corona. Nanoscale 10, 4167–4172. https://doi.org/10.1039/C7NR07450F

Chapman, R., Plakhoitnik, T., 2013. Background-free imaging of luminescent nanodiamonds using external magnetic field for contrast enhancement. Opt. Lett., OL 38, 1847–1849. https://doi.org/10.1364/OL.38.001847

Chatterjee, A., Serniak, N., Czerniecki, B.J., 2015. Sentinel Lymph Node Biopsy in Breast Cancer: A Work in Progress. The Cancer Journal 21, 7–10. https://doi.org/10.1097/PPO.0000000000000090

Chen, H., Shao, L., Li, Q., Wang, J., 2013. Gold nanorods and their plasmonic properties. Chem. Soc. Rev. 42, 2679–2724. https://doi.org/10.1039/C2CS35367A

Chen, J., Liu, M., Huang, Q., Jiang, R., Huang, H., Deng, F., Wen, Y., Tian, J., Zhang, X., Wei, Y., 2018. A novel light-induced ATRP for the preparation of water dispersible fluorescent nanodiamonds and their biological imaging applications. Ceramics International 44, 9907–9914. https://doi.org/10.1016/j.ceramint.2018.03.011

Chen, L.-Y., Wang, C.-W., Yuan, Z., Chang, H.-T., 2015. Fluorescent Gold Nanoclusters: Recent Advances in Sensing and Imaging. Anal. Chem. 87, 216–229. https://doi.org/10.1021/ac503636j

Chen, T., Yao, Q., Nasaruddin, R.R., Xie, J., 2019. Electrospray Ionization Mass Spectrometry: A Powerful Platform for Noble-Metal Nanocluster Analysis.

Angewandte Chemie International Edition 58, 11967–11977. https://doi.org/10.1002/anie.201901970

Chipaux, M., Laan, K.J. van der, Hemelaar, S.R., Hasani, M., Zheng, T., Schirhagl, R., 2018. Nanodiamonds and Their Applications in Cells. Small 14, 1704263. https://doi.org/10.1002/smll.201704263

Cilliers, C., Nessler, I., Christodolu, N., Thurber, G.M., 2017. Tracking Antibody Distribution with Near-Infrared Fluorescent Dyes: Impact of Dye Structure and Degree of Labeling on Plasma Clearance. Mol. Pharmaceutics 14, 1623–1633. https://doi.org/10.1021/acs.molpharmaceut.6b01091

Colombé, C., Le Guével, X., Martin-Serrano, A., Henry, M., Porret, E., Comby-Zerbino, C., Antoine, R., Atallah, I., Busser, B., Coll, J.-L., Righini, C.A., Sancey, L., 2019. Gold nanoclusters as a contrast agent for image-guided surgery of head and neck tumors. Nanomedicine: Nanotechnology, Biology and Medicine 20, 102011. https://doi.org/10.1016/j.nano.2019.04.014

Datta, R., Heaster, T.M., Sharick, J.T., Gillette, A.A., Skala, M.C., 2020. Fluorescence lifetime imaging microscopy: fundamentals and advances in instrumentation, analysis, and applications. J. Biomed. Opt. 25, 1. https://doi.org/10.1117/1.JBO.25.7.071203

David Nathanson, S., Anaya, P., Karvelis, K.C., Eck, L., Havstad, S., 1997. Sentinel lymph node uptake of two different technetium-labeled radiocolloids. Annals of Surgical Oncology 4, 104–110. https://doi.org/10.1007/BF02303791

Dei Cas, L., Zeldin, S., Nunn, N., Torelli, M., Shames, A.I., Zaitsev, A.M., Shenderova, O., 2019. Fluorescent Diamond Particles: From Fancy Blue to Red: Controlled Production of a Vibrant Color Spectrum of Fluorescent Diamond Particles (Adv. Funct. Mater. 19/2019). Adv. Funct. Mater. 29, 1970128. https://doi.org/10.1002/adfm.201970128

Deken, M.M., van Doorn, H.C., Verver, D., Boogerd, L.S.F., de Valk, K.S., Rietbergen, D.D.D., van Poelgeest, M.I.E., de Kroon, C.D., Beltman, J.J., van Leeuwen, F.W.B., Putter, H., Braak, J.P.B.M., de Geus-Oei, L.-F., van de Velde, C.J.H., Burggraaf, J., Vahrmeijer, A.L., Gaarenstroom, K.N., 2020. Near-infrared fluorescence imaging compared to standard sentinel lymph node detection with blue dye in patients with vulvar cancer – a randomized controlled trial. Gynecologic Oncology 159, 672–680. https://doi.org/10.1016/j.ygyno.2020.09.044

Dong, Y., Cao, R., Li, Y., Wang, Z., Li, L., Tian, L., 2015. Folate-conjugated nanodiamond for tumor-targeted drug delivery. RSC Adv. 5, 82711–82716. https://doi.org/10.1039/C5RA12383F

Dos Santos, T., Varela, J., Lynch, I., Salvati, A., Dawson, K.A., 2011. Quantitative Assessment of the Comparative Nanoparticle-Uptake Efficiency of a Range of Cell Lines. Small 7, 3341–3349. https://doi.org/10.1002/smll.201101076

Ehlerding, E.B., Chen, F., Cai, W., 2016. Biodegradable and Renal Clearable Inorganic Nanoparticles. Adv Sci (Weinh) 3, 1500223. https://doi.org/10.1002/advs.201500223

Farokhzad, O.C., Langer, R., 2009. Impact of Nanotechnology on Drug Delivery. ACS Nano 3, 16–20. https://doi.org/10.1021/nn900002m

Feng, Y., Li, K., Roth, E., Chao, D., Mecca, C.M., Hogan, Q.H., Pawela, C., Kwok, W.-M., Camara, A.K.S., Pan, B., 2021. Repetitive Mild Traumatic Brain Injury in Rats Impairs Cognition, Enhances Prefrontal Cortex Neuronal Activity, and Reduces Pre-synaptic Mitochondrial Function. Front. Cell. Neurosci. 15, 689334. https://doi.org/10.3389/fncel.2021.689334

Ferri, F., Montorfano, L., Bordes, S.J., Forleiter, C., Newman, M.I., 2021. Near-Infrared Fluorescence Imaging for Sentinel Lymph Node Identification in Melanoma Surgery. Cureus. https://doi.org/10.7759/cureus.14550

García De Abajo, F.J., Howie, A., 2002. Retarded field calculation of electron energy loss in inhomogeneous dielectrics. Phys. Rev. B 65, 115418. https://doi.org/10.1103/PhysRevB.65.115418

Girard, J.-P., Moussion, C., Förster, R., 2012. HEVs, lymphatics and homeostatic immune cell trafficking in lymph nodes. Nat Rev Immunol 12, 762–773. https://doi.org/10.1038/nri3298

Giuliano, A.E., Haigh, P.I., Brennan, M.B., Hansen, N.M., Kelley, M.C., Ye, W., Glass, E.C., Turner, R.R., 2000. Prospective Observational Study of Sentinel Lymphadenectomy Without Further Axillary Dissection in Patients With Sentinel Node–Negative Breast Cancer. JCO 18, 2553–2559. https://doi.org/10.1200/JCO.2000.18.13.2553

Giuliano, A.E., Kirgan, D.M., Guenther, J.M., Morton, D.L., 1994. Lymphatic Mapping and Sentinel Lymphadenectomy for Breast Cancer: Annals of Surgery 220, 391–401. https://doi.org/10.1097/00000658-199409000-00015

Gopika, G.S., Prasad, P.M.H., Lekshmi, A.G., Lekshmypriya, S., Sreesaila, S., Arunima, C., Kumar, M.S., Anil, A., Sreekumar, A., Pillai, Z.S., 2021. Chemistry of cyanine dyes-A review. Materials Today: Proceedings 46, 3102–3108. https://doi.org/10.1016/j.matpr.2021.02.622

Gould, E.A., Winship, T., Philbin, P.H., Kerr, H.H., 1960. Observations on a “sentinel node” in cancer of the parotid. Cancer 13, 77–78. https://doi.org/10.1002/1097-0142(196001/02)13:1<77::AID-CNCR2820130114>3.0.CO;2-D

Gray, E.E., Cyster, J.G., 2012. Lymph Node Macrophages. J Innate Immun 4, 424–436. https://doi.org/10.1159/000337007

Guarina, L., Calorio, C., Gavello, D., Moreva, E., Traina, P., Battiato, A., Ditalia Tchernij, S., Forneris, J., Gai, M., Picollo, F., Olivero, P., Genovese, M., Carbone, E., Marcantoni, A., Carabelli, V., 2018. Nanodiamonds-induced effects on neuronal firing of mouse hippocampal microcircuits. Scientific Reports 8, 1–14. https://doi.org/10.1038/s41598-018-20528-5

Gubala, V., Giovannini, G., Kunc, F., Monopoli, M.P., Moore, C.J., 2020. Dye-doped silica nanoparticles: synthesis, surface chemistry and bioapplications. Cancer Nano 11, 1. https://doi.org/10.1186/s12645-019-0056-x

Hada, A.-M., Craciun, A.-M., Astilean, S., 2021. Intrinsic Photoluminescence of Solid-State Gold Nanoclusters: Towards Fluorescence Lifetime Imaging of

Tissue-Like Phantoms Under Two-Photon Near-Infrared Excitation. Front. Chem. 9, 761711. https://doi.org/10.3389/fchem.2021.761711

Haigh, P.I., Hsueh, E.C., Giuliano, A.E., 1999. Sentinel lymphadenectomy in breast cancer. Breast Cancer 6, 139–144. https://doi.org/10.1007/BF02966922

Häkkinen, H., 2012. The gold–sulfur interface at the nanoscale. Nature Chem 4, 443–455. https://doi.org/10.1038/nchem.1352

Harrell, M.I., Iritani, B.M., Ruddell, A., 2007. Tumor-Induced Sentinel Lymph Node Lymphangiogenesis and Increased Lymph Flow Precede Melanoma Metastasis. The American Journal of Pathology 170, 774–786. https://doi.org/10.2353/ajpath.2007.060761

Haute, D.V., Berlin, J.M., 2017. Challenges in realizing selectivity for nanoparticle biodistribution and clearance: lessons from gold nanoparticles. Therapeutic Delivery 8, 763–774. https://doi.org/10.4155/tde-2017-0057

Hebels, E.R., Najafi, M., Van Den Dikkenberg, J., Beztsinna, N., Van De Looij, S., Wilbie, D., Meeldijk, J., Hembury, M., Vermonden, T., 2021. Luminescent gold nanocluster-decorated polymeric hybrid particles for laser guided therapy. European Polymer Journal 152, 110467. https://doi.org/10.1016/j.eurpolymj.2021.110467

Hembury, M., Chiappini, C., Bertazzo, S., Kalber, T.L., Drisko, G.L., Ogunlade, O., Walker-Samuel, S., Krishna, K.S., Jumeaux, C., Beard, P., Kumar, C.S.S.R., Porter, A.E., Lythgoe, M.F., Boissière, C., Sanchez, C., Stevens, M.M., 2015. Gold–silica quantum rattles for multimodal imaging and therapy. Proc. Natl. Acad. Sci. U.S.A. 112, 1959–1964. https://doi.org/10.1073/pnas.1419622112

Hsieh, F.-J., Sotoma, S., Lin, H.-H., Cheng, C.-Y., Yu, T.-Y., Hsieh, C.-L., Lin, C.-H., Chang, H.-C., 2019. Bioorthogonal Fluorescent Nanodiamonds for Continuous Long-Term Imaging and Tracking of Membrane Proteins. ACS Appl. Mater. Interfaces 11, 19774–19781. https://doi.org/10.1021/acsami.9b03640

Hu, D.-H., Sheng, Z.-H., Zhang, P.-F., Yang, D.-Z., Liu, S.-H., Gong, P., Gao, D.-Y., Fang, S.-T., Ma, Y.-F., Cai, L.-T., 2013. Hybrid gold–gadolinium nanoclusters for tumor-targeted NIRF/CT/MRI triple-modal imaging in vivo. Nanoscale 5, 1624. https://doi.org/10.1039/c2nr33543c

Hu, L., Zhang, Q., Li, X., Serpe, M.J., 2019. Stimuli-responsive polymers for sensing and actuation. Mater. Horiz. 6, 1774–1793. https://doi.org/10.1039/C9MH00490D

Hu, Y., Zhao, Z., Harmon, T., Pentel, P.R., Ehrich, M., Zhang, C., 2018. Paradox of PEGylation in fabricating hybrid nanoparticle-based nicotine vaccines. Biomaterials 182, 72–81. https://doi.org/10.1016/j.biomaterials.2018.08.015

Huang, Y., Fuksman, L., Zheng, J., 2018. Luminescence mechanisms of ultrasmall gold nanoparticles. Dalton Trans. 47, 6267–6273. https://doi.org/10.1039/C8DT00420J

Igarashi, R., Yoshinari, Y., Yokota, H., Sugi, T., Sugihara, F., Ikeda, K., Sumiya, H., Tsuji, S., Mori, I., Tochio, H., Harada, Y., Shirakawa, M., 2012. Real-Time

Background-Free Selective Imaging of Fluorescent Nanodiamonds in Vivo. Nano Lett. 12, 5726–5732. https://doi.org/10.1021/nl302979d

Jacques, S.L., 2013. Optical properties of biological tissues: a review. Phys. Med. Biol. 58, R37–R61. https://doi.org/10.1088/0031-9155/58/11/R37

Jin, R., Zeng, C., Zhou, M., Chen, Y., 2016. Atomically Precise Colloidal Metal Nanoclusters and Nanoparticles: Fundamentals and Opportunities. Chem. Rev. 116, 10346–10413. https://doi.org/10.1021/acs.chemrev.5b00703

Kadhim, R.J., Karsh, E.H., Taqi, Z.J., Jabir, M.S., 2021. Biocompatibility of gold nanoparticles: In-vitro and In-vivo study. Materials Today: Proceedings 42, 3041–3045. https://doi.org/10.1016/j.matpr.2020.12.826

Khatoon, S., Han, H., Jeon, J., Rao, N., Jeong, D.-W., Ikram, M., Yasin, T., Yi, G.-R., Park, J., 2018. Hypoxia-Responsive Mesoporous Nanoparticles for Doxorubicin Delivery. Polymers 10, 390. https://doi.org/10.3390/polym10040390

Kim, J.K., Jang, D.-J., 2017. Metal-enhanced fluorescence of gold nanoclusters adsorbed onto Ag@SiO $_2$ core–shell nanoparticles. J. Mater. Chem. C 5, 6037–6046. https://doi.org/10.1039/C7TC01352C

Kim, K.H., Nam, J., Choi, J., Seo, M., Bang, J., 2022. From macromonomers to bottlebrush copolymers with sequence control: synthesis, properties, and applications. Polym. Chem. 13, 2224–2261. https://doi.org/10.1039/D2PY00126H

Kohle, F.F.E., Hinckley, J.A., Wiesner, U.B., 2019. Dye Encapsulation in Fluorescent Core–Shell Silica Nanoparticles as Probed by Fluorescence Correlation Spectroscopy. J. Phys. Chem. C 123, 9813–9823. https://doi.org/10.1021/acs.jpcc.9b00297

Krag, D.N., Anderson, S.J., Julian, T.B., Brown, A.M., Harlow, S.P., Ashikaga, T., Weaver, D.L., Miller, B.J., Jalovec, L.M., Frazier, T.G., Noyes, R.D., Robidoux, A., Scarth, H.M., Mammolito, D.M., McCready, D.R., Mamounas, E.P., Costantino, J.P., Wolmark, N., 2007. Technical outcomes of sentinel-lymph-node resection and conventional axillary-lymph-node dissection in patients with clinically node-negative breast cancer: results from the NSABP B-32 randomised phase III trial. The Lancet Oncology 8, 881–888. https://doi.org/10.1016/S1470-2045(07)70278-4

Krag, D.N., Anderson, S.J., Julian, T.B., Brown, A.M., Harlow, S.P., Costantino, J.P., Ashikaga, T., Weaver, D.L., Mamounas, E.P., Jalovec, L.M., Frazier, T.G., Noyes, R.D., Robidoux, A., Scarth, H.M., Wolmark, N., 2010. Sentinel-lymph-node resection compared with conventional axillary-lymph-node dissection in clinically node-negative patients with breast cancer: overall survival findings from the NSABP B-32 randomised phase 3 trial. The Lancet Oncology 11, 927–933. https://doi.org/10.1016/S1470-2045(10)70207-2

Krag, D.N., Weaver, D.L., Alex, J.C., Fairbank, J.T., 1993. Surgical resection and radiolocalization of the sentinel lymph node in breast cancer using a gamma probe. Surgical Oncology 2, 335–340. https://doi.org/10.1016/0960-7404(93)90064-6

Krueger, A., 2017. Current issues and challenges in surface chemistry of nanodiamonds, in: Nanodiamonds. Elsevier, pp. 183–242. https://doi.org/10.1016/B978-0-32-343029-6.00008-8

Kuehn, T., Bauerfeind, I., Fehm, T., Fleige, B., Hausschild, M., Helms, G., Lebeau, A., Liedtke, C., Minckwitz, G.V., Nekljudova, V., Schmatloch, S., Schrenk, P., Staebler, A., Untch, M., 2013. Sentinel-lymph-node biopsy in patients with breast cancer before and after neoadjuvant chemotherapy (SENTINA): a prospective, multicentre cohort study. The Lancet Oncology 14, 609–618. https://doi.org/10.1016/S1470-2045(13)70166-9

Kuhn, D.A., Vanhecke, D., Michen, B., Blank, F., Gehr, P., Petri-Fink, A., Rothen-Rutishauser, B., 2014. Different endocytotic uptake mechanisms for nanoparticles in epithelial cells and macrophages. Beilstein J. Nanotechnol. 5, 1625–1636. https://doi.org/10.3762/bjnano.5.174

Kumar, A., Das, N., Rayavarapu, R.G., 2023. Role of Tunable Gold Nanostructures in Cancer Nanotheranostics: Implications on Synthesis, Toxicity, Clinical Applications and Their Associated Opportunities and Challenges. JNT 4, 1–34. https://doi.org/10.3390/jnt4010001

Kumar, C.S.S.R., 2009. Nanomaterials for the life science. Volume 3, Volume 3,. Wiley-VCH, Weinheim.

Kuwahata, A., Tanaka, R., Matsuda, S., Amada, E., Irino, T., Mayanagi, S., Chikaki, S., Saito, I., Tanabe, N., Kawakubo, H., Takeuchi, H., Kitagawa, Y., Kusakabe, M., Sekino, M., 2020. Development of Magnetic Probe for Sentinel Lymph Node Detection in Laparoscopic Navigation for Gastric Cancer Patients. Sci Rep 10, 1798. https://doi.org/10.1038/s41598-020-58530-5

Kvakova, K., Ondra, M., Schimer, J., Petrik, M., Novy, Z., Raabova, H., Hajduch, M., Cigler, P., 2022. Visualization of Sentinel Lymph Nodes with Mannosylated Fluorescent Nanodiamonds. Advanced Functional Materials 32, 2109960. https://doi.org/10.1002/adfm.202109960

Kwak, K., Thanthirige, V.D., Pyo, K., Lee, D., Ramakrishna, G., 2017. Energy Gap Law for Exciton Dynamics in Gold Cluster Molecules. J. Phys. Chem. Lett. 8, 4898–4905. https://doi.org/10.1021/acs.jpclett.7b01892

Laissue, P.P., Alghamdi, R.A., Tomancak, P., Reynaud, E.G., Shroff, H., 2017. Assessing phototoxicity in live fluorescence imaging. Nat Methods 14, 657–661. https://doi.org/10.1038/nmeth.4344

Lakowicz, J.R., 2009. Principles of Fluorescence Spectroscopy. Springer.

Lambrou, N.C., Amadeo, A., 2021. Surgical Gynecologic Oncology, in: Breast Cancer and Gynecologic Cancer Rehabilitation. Elsevier, pp. 171–188. https://doi.org/10.1016/B978-0-323-72166-0.00018-9

Li, H.-C., Hsieh, F.-J., Chen, C.-P., Chang, M.-Y., Hsieh, P.C.H., Chen, C.-C., Hung, S.-U., Wu, C.-C., Chang, H.-C., 2013. The hemocompatibility of oxidized diamond nanocrystals for biomedical applications. Scientific Reports 3. https://doi.org/10.1038/srep03044

Li, Huili, Li, Hongle, Wan, A., 2020. Luminescent gold nanoclusters for *in vivo* tumor imaging. Analyst 145, 348–363. https://doi.org/10.1039/C9AN01598A

Liu, J.-M., Chen, J.-T., Yan, X.-P., 2013. Near Infrared Fluorescent Trypsin Stabilized Gold Nanoclusters as Surface Plasmon Enhanced Energy Transfer Biosensor and in Vivo Cancer Imaging Bioprobe. Anal. Chem. 85, 3238–3245. https://doi.org/10.1021/ac303603f

Liu, N., Tang, M., 2020. Toxicity of different types of quantum dots to mammalian cells in vitro: An update review. Journal of Hazardous Materials 399, 122606. https://doi.org/10.1016/j.jhazmat.2020.122606

Louie, D.A.P., Liao, S., 2019. Lymph Node Subcapsular Sinus Macrophages as the Frontline of Lymphatic Immune Defense. Front. Immunol. 10, 347. https://doi.org/10.3389/fimmu.2019.00347

Luo, L., Liu, Z., Du, X., Jin, R., 2023. Photoluminescence of the Au38(SR)26 nanocluster comprises three radiative processes. Commun Chem 6, 22. https://doi.org/10.1038/s42004-023-00819-3

Magidson, V., Khodjakov, A., 2013. Circumventing Photodamage in Live-Cell Microscopy, in: Methods in Cell Biology. Elsevier, pp. 545–560. https://doi.org/10.1016/B978-0-12-407761-4.00023-3

Maziukiewicz, D., Grześkowiak, B., Coy, E., Jurga, S., Mrówczyński, R., 2019. NDs@PDA@ICG Conjugates for Photothermal Therapy of Glioblastoma Multiforme. Biomimetics 4, 3. https://doi.org/10.3390/biomimetics4010003

McHugh, K.J., Jing, L., Behrens, A.M., Jayawardena, S., Tang, W., Gao, M., Langer, R., Jaklenec, A., 2018. Biocompatible Semiconductor Quantum Dots as Cancer Imaging Agents. Adv. Mater. 30, 1706356. https://doi.org/10.1002/adma.201706356

Mertens, H., Koenderink, A.F., Polman, A., 2007. Plasmon-enhanced luminescence near noble-metal nanospheres: Comparison of exact theory and an improved Gersten and Nitzan model. Phys. Rev. B 76, 115123. https://doi.org/10.1103/PhysRevB.76.115123

Mettler, F.A., Guiberteau, M.J., 2019. Essentials of nuclear medicine and molecular imaging, 7th edition. ed. Elsevier, Philadelphia, PA.

Meyer, S.M., Murphy, C.J., 2022. Anisotropic silica coating on gold nanorods boosts their potential as SERS sensors. Nanoscale 14, 5214–5226. https://doi.org/10.1039/D1NR07918B

Mishra, D., Aldeek, F., Lochner, E., Palui, G., Zeng, B., Mackowski, S., Mattoussi, H., 2016. Aqueous Growth of Gold Clusters with Tunable Fluorescence Using Photochemically Modified Lipoic Acid-Based Ligands. Langmuir 32, 6445–6458. https://doi.org/10.1021/acs.langmuir.6b00950

Mitura, K.A., Włodarczyk, E., 2018. Fluorescent Nanodiamonds in Biomedical Applications. Journal of AOAC INTERNATIONAL 101, 1297–1307. https://doi.org/10.5740/jaoacint.18-0044

Monici, M., 2005. Cell and tissue autofluorescence research and diagnostic applications, in: Biotechnology Annual Review. Elsevier, pp. 227–256. https://doi.org/10.1016/S1387-2656(05)11007-2

Moran, I., Grootveld, A.K., Nguyen, A., Phan, T.G., 2019. Subcapsular Sinus Macrophages: The Seat of Innate and Adaptive Memory in Murine Lymph Nodes. Trends in Immunology 40, 35–48. https://doi.org/10.1016/j.it.2018.11.004

Morton, D.L., 1992. Technical Details of Intraoperative Lymphatic Mapping for Early Stage Melanoma. Arch Surg 127, 392. https://doi.org/10.1001/archsurg.1992.01420040034005

Morton, D.L., Thompson, J.F., Cochran, A.J., Mozzillo, N., Elashoff, R., Essner, R., Nieweg, O.E., Roses, D.F., Hoekstra, H.J., Karakousis, C.P., Reintgen, D.S., Coventry, B.J., Glass, E.C., Wang, H.-J., 2006. Sentinel-Node Biopsy or Nodal Observation in Melanoma. N Engl J Med 355, 1307–1317. https://doi.org/10.1056/NEJMoa060992

Muhammed, M.A.H., Ramesh, S., Sinha, S.S., Pal, S.K., Pradeep, T., 2010. Two distinct fluorescent quantum clusters of gold starting from metallic nanoparticles by pH-dependent ligand etching. Nano Res. 1, 333–340. https://doi.org/10.1007/s12274-008-8035-2

Murphy, K., Weaver, C., 2016. Janeway's immunobiology, 9th edition. ed. Garland Science/Taylor & Francis Group, LLC, New York, NY.

Nadal, C., Coutelier, O., Cavalie, S., Flaud, V., Soulié, J., Marty, J.-D., Destarac, M., Tourrette, A., 2022. Polymer/silica core–shell nanoparticles with temperature-dependent stability properties. European Polymer Journal 168, 111104. https://doi.org/10.1016/j.eurpolymj.2022.111104

Nagaya, T., Nakamura, Y.A., Choyke, P.L., Kobayashi, H., 2017. Fluorescence-Guided Surgery. Front. Oncol. 7, 314. https://doi.org/10.3389/fonc.2017.00314

Nair, L.V., Nazeer, S.S., Jayasree, R.S., Ajayaghosh, A., 2015. Fluorescence Imaging Assisted Photodynamic Therapy Using Photosensitizer-Linked Gold Quantum Clusters. ACS Nano 9, 5825–5832. https://doi.org/10.1021/acsnano.5b00406

Namdari, P., Negahdari, B., Eatemadi, A., 2017. Synthesis, properties and biomedical applications of carbon-based quantum dots: An updated review. Biomedicine & Pharmacotherapy 87, 209–222. https://doi.org/10.1016/j.biopha.2016.12.108

Namikawa, T., 2015. Clinical applications of 5-aminolevulinic acid-mediated fluorescence for gastric cancer. WJG 21, 8769. https://doi.org/10.3748/wjg.v21.i29.8769

Neburkova, J., Hajek, M., Rehor, I., Schimer, J., Sedlak, F., Stursa, J., Hruby, M., Cigler, P., 2018a. Targeting Glioma Cancer Cells with Fluorescent Nanodiamonds via Integrin Receptors, in: Integrin Targeting Systems for Tumor Diagnosis and Therapy, Methods in Pharmacology and Toxicology. Humana Press, pp. 169–189. https://doi.org/10.1007/7653_2017_68

Neburkova, J., Sedlak, F., Zackova Suchanova, J., Kostka, L., Sacha, P., Subr, V., Etrych, T., Simon, P., Barinkova, J., Krystufek, R., Spanielova, H., Forstova, J., Konvalinka, J., Cigler, P., 2018b. Inhibitor–GCPII Interaction: Selective and Robust System for Targeting Cancer Cells with Structurally Diverse Nanoparticles. Mol. Pharmaceutics 15, 2932–2945. https://doi.org/10.1021/acs.molpharmaceut.7b00889

Neburkova, J., Vavra, J., Cigler, P., 2017. Coating nanodiamonds with biocompatible shells for applications in biology and medicine. Current Opinion in Solid State and Materials Science 21, 43–53. https://doi.org/10.1016/j.cossms.2016.05.008

Nikoobakht, B., El-Sayed, M.A., 2003. Preparation and Growth Mechanism of Gold Nanorods (NRs) Using Seed-Mediated Growth Method. Chem. Mater. 15, 1957–1962. https://doi.org/10.1021/cm020732l

Ntziachristos, V., 2010. Going deeper than microscopy: the optical imaging frontier in biology. Nat Methods 7, 603–614. https://doi.org/10.1038/nmeth.1483

Nunn, N., Torelli, M., McGuire, G., Shenderova, O., 2017. Nanodiamond: A high impact nanomaterial. Current Opinion in Solid State and Materials Science, Nanodiamond Science and Technology 21, 1–9. https://doi.org/10.1016/j.cossms.2016.06.008

Oh, E., Fatemi, F.K., Currie, M., Delehanty, J.B., Pons, T., Fragola, A., Lévêque-Fort, S., Goswami, R., Susumu, K., Huston, A.L., Medintz, I.L., 2013. PEGylated Luminescent Gold Nanoclusters: Synthesis, Characterization, Bioconjugation, and Application to One- and Two-Photon Cellular Imaging. Part. Part. Syst. Charact. 30, 453–466. https://doi.org/10.1002/ppsc.201200140

Oh, E., Susumu, K., Goswami, R., Mattoussi, H., 2010. One-Phase Synthesis of Water-Soluble Gold Nanoparticles with Control over Size and Surface Functionalities. Langmuir 26, 7604–7613. https://doi.org/10.1021/la904438s

Pang, Z., Yan, W., Yang, J., Li, Q., Guo, Y., Zhou, D., Jiang, X., 2022. Multifunctional Gold Nanoclusters for Effective Targeting, Near-Infrared Fluorescence Imaging, Diagnosis, and Treatment of Cancer Lymphatic Metastasis. ACS Nano 16, 16019–16037. https://doi.org/10.1021/acsnano.2c03752

Pavelka, O., Dyakov, S., Veselý, J., Fučíková, A., Sugimoto, H., Fujii, M., Valenta, J., 2021. Optimizing plasmon enhanced luminescence in silicon nanocrystals by gold nanorods. Nanoscale 13, 5045–5057. https://doi.org/10.1039/D1NR00058F

Pavelka, O., Dyakov, S.A., Kvakova, K., Vesely, J., Cigler, P., Valenta, J., 2023. Towards Site-Specific Emission Enhancement of Gold Nanoclusters Using Plasmonic Systems: Advantages and Limitations. Nanoscale 10.1039.D2NR06680G. https://doi.org/10.1039/D2NR06680G

Pavelka, O., Kvakova, K., Vesely, J., Mizera, J., Cigler, P., Valenta, J., 2022. Optically coupled gold nanostructures: plasmon enhanced luminescence from gold nanorod-nanocluster hybrids. Nanoscale 14, 3166–3178. https://doi.org/10.1039/D1NR08254J

Petrini, G., Tomagra, G., Bernardi, E., Moreva, E., Traina, P., Marcantoni, A., Picollo, F., Kvaková, K., Cígler, P., Degiovanni, I.P., Carabelli, V., Genovese, M., 2022. Nanodiamond–Quantum Sensors Reveal Temperature Variation Associated to Hippocampal Neurons Firing. Advanced Science 9, 2202014. https://doi.org/10.1002/advs.202202014

Piscatelli, N., Crawford, S., Larkin, A., Robert, Q., Layeequr Rahman, R., 2009. Complications of methylene blue dye infiltration for sentinel lymph node biopsy in breast cancer. Cancer Research 69, 4140. https://doi.org/10.1158/0008-5472.SABCS-4140

Pohanka, M., 2017. Quantum Dots in the Therapy: Current Trends and Perspectives. MRMC 17, 650–656. https://doi.org/10.2174/1389557517666170120153342

Porret, E., Le Guével, X., Coll, J.-L., 2020. Gold nanoclusters for biomedical applications: toward *in vivo* studies. J. Mater. Chem. B 8, 2216–2232. https://doi.org/10.1039/C9TB02767J

Porret, E., Sancey, L., Martín-Serrano, A., Montañez, M.I., Seeman, R., Yahia-Ammar, A., Okuno, H., Gomez, F., Ariza, A., Hildebrandt, N., Fleury, J.-B., Coll, J.-L., Le Guével, X., 2017. Hydrophobicity of Gold Nanoclusters Influences Their Interactions with Biological Barriers. Chem. Mater. 29, 7497–7506. https://doi.org/10.1021/acs.chemmater.7b02497

Pouw, J.J., Grootendorst, M.R., Bezooijen, R., Klazen, C.A.H., De Bruin, W.I., Klaase, J.M., Hall-Craggs, M.A., Douek, M., Ten Haken, B., 2015. Pre-operative sentinel lymph node localization in breast cancer with superparamagnetic iron oxide MRI: the SentiMAG Multicentre Trial imaging subprotocol. BJR 88, 20150634. https://doi.org/10.1259/bjr.20150634

Pramanik, G., Humpolickova, J., Valenta, J., Kundu, P., Bals, S., Bour, P., Dracinsky, M., Cigler, P., 2018. Gold nanoclusters with bright near-infrared photoluminescence. Nanoscale 10, 3792–3798. https://doi.org/10.1039/C7NR06050E

Pramanik, G., Keprova, A., Valenta, J., Bocan, V., Kvaková, K., Libusova, L., Cigler, P., 2020. Synthesis of Near-Infrared Emitting Gold Nanoclusters for Biological Applications. J. Vis. Exp. 157, e60388. https://doi.org/10.3791/60388

Pramanik, G., Kvakova, K., Thottappali, M.A., Rais, D., Pfleger, J., Greben, M., El-Zoka, A., Bals, S., Dracinsky, M., Valenta, J., Cigler, P., 2021. Inverse heavy-atom effect in near infrared photoluminescent gold nanoclusters. Nanoscale 13, 10462–10467. https://doi.org/10.1039/D1NR02440J

Qian, H., Jiang, D., Li, G., Gayathri, C., Das, A., Gil, R.R., Jin, R., 2012. Monoplatinum Doping of Gold Nanoclusters and Catalytic Application. J. Am. Chem. Soc. 134, 16159–16162. https://doi.org/10.1021/ja307657a

Qin, H., Ma, D., Du, J., 2018a. Distance dependent fluorescence quenching and enhancement of gold nanoclusters by gold nanoparticles. Spectrochimica Acta Part A: Molecular and Biomolecular Spectroscopy 189, 161–166. https://doi.org/10.1016/j.saa.2017.08.025

Qin, H., Ma, D., Du, J., 2018b. Distance dependent fluorescence quenching and enhancement of gold nanoclusters by gold nanoparticles. Spectrochimica Acta Part A: Molecular and Biomolecular Spectroscopy 189, 161–166. https://doi.org/10.1016/j.saa.2017.08.025

Qin, J.-X., Yang, X.-G., Lv, C.-F., Li, Y.-Z., Liu, K.-K., Zang, J.-H., Yang, X., Dong, L., Shan, C.-X., 2021. Nanodiamonds: Synthesis, properties, and applications in nanomedicine. Materials & Design 210, 110091. https://doi.org/10.1016/j.matdes.2021.110091

Qin, L., He, X., Chen, L., Zhang, Y., 2015. Turn-on Fluorescent Sensing of Glutathione *S* -Transferase at near-Infrared Region Based on FRET between Gold Nanoclusters and Gold Nanorods. ACS Appl. Mater. Interfaces 7, 5965–5971. https://doi.org/10.1021/acsami.5b00269

Refaat, A., Yap, M.L., Pietersz, G., Walsh, A.P.G., Zeller, J., Del Rosal, B., Wang, X., Peter, K., 2022. In vivo fluorescence imaging: success in preclinical imaging paves the way for clinical applications. J Nanobiotechnol 20, 450. https://doi.org/10.1186/s12951-022-01648-7

Rehor, I., Slegerova, J., Kucka, J., Proks, V., Petrakova, V., Adam, M.-P., Treussart, F., Turner, S., Bals, S., Sacha, P., Ledvina, M., Wen, A.M., Steinmetz, N.F., Cigler, P., 2014. Fluorescent Nanodiamonds: Fluorescent Nanodiamonds Embedded in Biocompatible Translucent Shells (Small 6/2014). Small 10, 1029–1029. https://doi.org/10.1002/smll.201470033

Reineck, P., Francis, A., Orth, A., Lau, D.W.M., Nixon-Luke, R.D.V., Rastogi, I.D., Razali, W.A.W., Cordina, N.M., Parker, L.M., Sreenivasan, V.K.A., Brown, L.J., Gibson, B.C., 2016. Brightness and Photostability of Emerging Red and Near-IR Fluorescent Nanomaterials for Bioimaging. Advanced Optical Materials 4, 1549–1557. https://doi.org/10.1002/adom.201600212

Reineck, P., Trindade, L.F., Havlik, J., Stursa, J., Heffernan, A., Elbourne, A., Orth, A., Capelli, M., Cigler, P., Simpson, D.A., Gibson, B.C., 2019. Not All Fluorescent Nanodiamonds Are Created Equal: A Comparative Study. Particle & Particle Systems Characterization 36, 1900009. https://doi.org/10.1002/ppsc.201900009

Reisch, A., Klymchenko, A.S., 2016. Fluorescent Polymer Nanoparticles Based on Dyes: Seeking Brighter Tools for Bioimaging. Small 12, 1968–1992. https://doi.org/10.1002/smll.201503396

Segawa, T.F., Igarashi, R., 2023. Nanoscale quantum sensing with Nitrogen-Vacancy centers in nanodiamonds – A magnetic resonance perspective. Progress in Nuclear Magnetic Resonance Spectroscopy 134–135, 20–38. https://doi.org/10.1016/j.pnmrs.2022.12.001

Servais, E.L., Colovos, C., Bograd, A.J., White, J., Sadelain, M., Adusumilli, P.S., 2011. Animal models and molecular imaging tools to investigate lymph node metastases. J Mol Med 89, 753–769. https://doi.org/10.1007/s00109-011-0764-0

Shang, L., Dong, S., Nienhaus, G.U., 2011. Ultra-small fluorescent metal nanoclusters: Synthesis and biological applications. Nano Today 6, 401–418. https://doi.org/10.1016/j.nantod.2011.06.004

Shang, L., Nienhaus, G.U., 2012. Gold nanoclusters as novel optical probes for in vitro and in vivo fluorescence imaging. Biophys Rev 4, 313–322. https://doi.org/10.1007/s12551-012-0076-9

Shang, L., Stockmar, F., Azadfar, N., Nienhaus, G.U., 2013. Intracellular Thermometry by Using Fluorescent Gold Nanoclusters. Angew. Chem. Int. Ed. 52, 11154–11157. https://doi.org/10.1002/anie.201306366

Shenderova, O.A., McGuire, G.E., 2015. Science and engineering of nanodiamond particle surfaces for biological applications (Review). Biointerphases 10, 030802. https://doi.org/10.1116/1.4927679

Shenoy, D., Fu, W., Li, J., Crasto, C., Jones, G., DiMarzio, C., Sridhar, S., Amiji, M., 2006. Surface functionalization of gold nanoparticles using hetero-bifunctional poly(ethylene glycol) spacer for intracellular tracking and delivery. International Journal of Nanomedicine 1, 51–58. https://doi.org/10.2147/nano.2006.1.1.51

Shi, Y., Liu, M., Wang, K., Huang, H., Wan, Q., Tao, L., Fu, L., Zhang, X., Wei, Y., 2015. Direct surface PEGylation of nanodiamond via RAFT polymerization. Applied Surface Science 357, Part B, 2147–2153. https://doi.org/10.1016/j.apsusc.2015.09.200

Slegerova, J., Hajek, M., Rehor, I., Sedlak, F., Stursa, J., Hruby, M., Cigler, P., 2015. Designing the nanobiointerface of fluorescent nanodiamonds: highly selective targeting of glioma cancer cells. Nanoscale 7, 415–420. https://doi.org/10.1039/C4NR02776K

Sreedhar, S., Maloney, J., Hudson, S., 2021. Introducing SENTIMAG in a rural setting: a 5-year experience. ANZ Journal of Surgery 91, 2404–2410. https://doi.org/10.1111/ans.17093

Stamplecoskie, K.G., Kamat, P.V., 2014. Size-Dependent Excited State Behavior of Glutathione-Capped Gold Clusters and Their Light-Harvesting Capacity. J. Am. Chem. Soc. 136, 11093–11099. https://doi.org/10.1021/ja505361n

Stummer, W., Pichlmeier, U., Meinel, T., Wiestler, O.D., Zanella, F., Reulen, H.-J., 2006. Fluorescence-guided surgery with 5-aminolevulinic acid for resection of malignant glioma: a randomised controlled multicentre phase III trial. The Lancet Oncology 7, 392–401. https://doi.org/10.1016/S1470-2045(06)70665-9

Sugie, T., Ikeda, T., Kawaguchi, A., Shimizu, A., Toi, M., 2017. Sentinel lymph node biopsy using indocyanine green fluorescence in early-stage breast cancer: a meta-analysis. Int J Clin Oncol 22, 11–17. https://doi.org/10.1007/s10147-016-1064-z

Taylor, M.E., Drickamer, K., 1993. Structural requirements for high affinity binding of complex ligands by the macrophage mannose receptor. J Biol Chem 268, 399–404.

Teshome, M., Wei, C., Hunt, K.K., Thompson, A., Rodriguez, K., Mittendorf, E.A., 2016. Use of a Magnetic Tracer for Sentinel Lymph Node Detection in Early-Stage Breast Cancer Patients: A Meta-analysis. Ann Surg Oncol 23, 1508–1514. https://doi.org/10.1245/s10434-016-5135-1

Tobis, S., Knopf, J., Silvers, C., Yao, J., Rashid, H., Wu, G., Golijanin, D., 2011. Near Infrared Fluorescence Imaging With Robotic Assisted Laparoscopic Partial Nephrectomy: Initial Clinical Experience for Renal Cortical Tumors. Journal of Urology 186, 47–52. https://doi.org/10.1016/j.juro.2011.02.2701

Tomczak, N., Liu, R., Vancso, J.G., 2013. Polymer-coated quantum dots. Nanoscale 5, 12018. https://doi.org/10.1039/c3nr03949h

Treussart, F., Vlasov, I.I., 2017. Photoluminescence of color centers in nanodiamonds, in: Nanodiamonds. Elsevier, pp. 155–181. https://doi.org/10.1016/B978-0-32-343029-6.00007-6

Trevaskis, N.L., Kaminskas, L.M., Porter, C.J.H., 2015. From sewer to saviour — targeting the lymphatic system to promote drug exposure and activity. Nat Rev Drug Discov 14, 781–803. https://doi.org/10.1038/nrd4608

Tuchin, V., 2007. Tissue Optics. SPIE, 1000 20th Street, Bellingham, WA 98227-0010 USA. https://doi.org/10.1117/3.684093

Turner, R.R., Ollila, D.W., Krasne, D.L., Giuliano, A.E., 1997. Histopathologic Validation of the Sentinel Lymph Node Hypothesis for Breast Carcinoma: Annals of Surgery 226, 271–278. https://doi.org/10.1097/00000658-199709000-00006

Turner, S., 2017. Structure, shape, defects and impurities in nanodiamonds investigated by HRTEM and STEM-EELS, in: Nanodiamonds. Elsevier, pp. 57–84. https://doi.org/10.1016/B978-0-32-343029-6.00003-9

Vahrmeijer, A.L., Hutteman, M., Van Der Vorst, J.R., Van De Velde, C.J.H., Frangioni, J.V., 2013. Image-guided cancer surgery using near-infrared fluorescence. Nat Rev Clin Oncol 10, 507–518. https://doi.org/10.1038/nrclinonc.2013.123

Vaijayanthimala, V., Cheng, P.-Y., Yeh, S.-H., Liu, K.-K., Hsiao, C.-H., Chao, J.-I., Chang, H.-C., 2012. The long-term stability and biocompatibility of fluorescent nanodiamond as an in vivo contrast agent. Biomaterials 33, 7794–7802. https://doi.org/10.1016/j.biomaterials.2012.06.084

Valenta, J., Greben, M., Pramanik, G., Kvakova, K., Cigler, P., 2021. Reversible photo- and thermal-effects on the luminescence of gold nanoclusters: implications for nanothermometry. Phys. Chem. Chem. Phys. 23, 11954–11960. https://doi.org/10.1039/D0CP06467J

Valeur, B., Berberan-Santos, M.N., 2012. Molecular Fluorescence: Principles and Applications, 1st ed. Wiley. https://doi.org/10.1002/9783527650002

Van De Looij, S.M., Hebels, E.R., Viola, M., Hembury, M., Oliveira, S., Vermonden, T., 2022. Gold Nanoclusters: Imaging, Therapy, and Theranostic Roles in Biomedical Applications. Bioconjugate Chem. 33, 4–23. https://doi.org/10.1021/acs.bioconjchem.1c00475

Van Manen, L., Handgraaf, H.J.M., Diana, M., Dijkstra, J., Ishizawa, T., Vahrmeijer, A.L., Mieog, J.S.D., 2018. A practical guide for the use of indocyanine green and methylene blue in fluorescence-guided abdominal surgery. J Surg Oncol 118, 283–300. https://doi.org/10.1002/jso.25105

Verbij, F.C., Sorvillo, N., Kaijen, P.H.P., Hrdinova, J., Peyron, I., Fijnheer, R., Ten Brinke, A., Meijer, A.B., Van Alphen, F.P.J., Van Den Berg, T.K., Graversen, J.J.H., Moestrup, S.K., Voorberg, J., 2017. The class I scavenger receptor CD163 promotes internalization of ADAMTS13 by macrophages. Blood Advances 1, 293–305. https://doi.org/10.1182/bloodadvances.2016001321

Veronesi, U., Viale, G., Paganelli, G., Zurrida, S., Luini, A., Galimberti, V., Veronesi, P., Intra, M., Maisonneuve, P., Zucca, F., Gatti, G., Mazzarol, G., De Cicco, C., Vezzoli, D., 2010. Sentinel Lymph Node Biopsy in Breast Cancer: Ten-Year Results of a Randomized Controlled Study. Annals of Surgery 251, 595–600. https://doi.org/10.1097/SLA.0b013e3181c0e92a

Villamena, F.A., 2017. Fluorescence Technique, in: Reactive Species Detection in Biology. Elsevier, pp. 87–162. https://doi.org/10.1016/B978-0-12-420017-3.00003-7

Wagner, A.M., Knipe, J.M., Orive, G., Peppas, N.A., 2019. Quantum dots in biomedical applications. Acta Biomaterialia 94, 44–63. https://doi.org/10.1016/j.actbio.2019.05.022

Wang, S., Meng, X., Das, A., Li, T., Song, Y., Cao, T., Zhu, X., Zhu, M., Jin, R., 2014. A 200-fold Quantum Yield Boost in the Photoluminescence of Silver-Doped AgxAu25−x Nanoclusters: The 13 th Silver Atom Matters. Angew. Chem. Int. Ed. 53, 2376–2380. https://doi.org/10.1002/anie.201307480

Waters, J.C., Wittmann, T., 2014. Concepts in quantitative fluorescence microscopy, in: Methods in Cell Biology. Elsevier, pp. 1–18. https://doi.org/10.1016/B978-0-12-420138-5.00001-X

Wei, M., Tian, Y., Wang, L., Hong, Y., Luo, D., Sha, Y., 2021. The Emission Mechanism of Gold Nanoclusters Capped with 11-Mercaptoundecanoic Acid, and the Detection of Methanol in Adulterated Wine Model. Materials 14, 6342. https://doi.org/10.3390/ma14216342

Wellens, L.M., Deken, M.M., Sier, C.F.M., Johnson, H.R., De La Jara Ortiz, F., Bhairosingh, S.S., Houvast, R.D., Kholosy, W.M., Baart, V.M., Pieters, A.M.M.J., De Krijger, R.R., Molenaar, J.J., Wehrens, E.J., Dekkers, J.F., Wijnen, M.H.W.A., Vahrmeijer, A.L., Rios, A.C., 2020. Anti-GD2-IRDye800CW as a targeted probe for fluorescence-guided surgery in neuroblastoma. Sci Rep 10, 17667. https://doi.org/10.1038/s41598-020-74464-4

Wilson, E.R., Parker, L.M., Orth, A., Nunn, N., Torelli, M., Shenderova, O., Gibson, B.C., Reineck, P., 2019. The effect of particle size on nanodiamond fluorescence and colloidal properties in biological media. Nanotechnology 30, 385704. https://doi.org/10.1088/1361-6528/ab283d

Wu, T.-J., Tzeng, Y.-K., Chang, W.-W., Cheng, C.-A., Kuo, Y., Chien, C.-H., Chang, H.-C., Yu, J., 2013. Tracking the engraftment and regenerative capabilities of transplanted lung stem cells using fluorescent nanodiamonds. Nat Nano 8, 682–689. https://doi.org/10.1038/nnano.2013.147

Wu, Z., Jin, R., 2010. On the Ligand’s Role in the Fluorescence of Gold Nanoclusters. Nano Lett. 10, 2568–2573. https://doi.org/10.1021/nl101225f

Xie, J., Zheng, Y., Ying, J.Y., 2009. Protein-Directed Synthesis of Highly Fluorescent Gold Nanoclusters. J. Am. Chem. Soc. 131, 888–889. https://doi.org/10.1021/ja806804u

Xu, P., Qiu, Q., Ye, X., Wei, M., Xi, W., Feng, H., Qian, Z., 2019. Halogenated tetraphenylethene with enhanced aggregation-induced emission: an anomalous anti-heavy-atom effect and self-reversible mechanochromism. Chem. Commun. 55, 14938–14941. https://doi.org/10.1039/C9CC07045A

Yadav, Y., Owens, E., Nomura, S., Fukuda, T., Baek, Y., Kashiwagi, S., Choi, H.S., Henary, M., 2020. Ultrabright and Serum-Stable Squaraine Dyes. J. Med. Chem. 63, 9436–9445. https://doi.org/10.1021/acs.jmedchem.0c00617

Yahia-Ammar, A., Sierra, D., Mérola, F., Hildebrandt, N., Le Guével, X., 2016. Self-Assembled Gold Nanoclusters for Bright Fluorescence Imaging and Enhanced Drug Delivery. ACS Nano 10, 2591–2599. https://doi.org/10.1021/acsnano.5b07596

Yang, D., Li, X., Zhou, W., Zhang, S., Meng, C., Wu, Y., Wang, Y., Zeng, H., 2019. $CsPbBr_3$ Quantum Dots 2.0: Benzenesulfonic Acid Equivalent Ligand Awakens Complete Purification. Adv. Mater. 1900767. https://doi.org/10.1002/adma.201900767

Yang, L.-X., Liu, Y.-C., Cho, C.-H., Chen, Y.-R., Yang, C.-S., Lu, Y.-L., Zhang, Z., Tsai, Y.-T., Chin, Y.-C., Yu, J., Pan, H.-M., Jiang, W.-R., Chia, Z.-C., Huang, W.-S., Chiu, Y.-L., Sun, C.-K., Huang, Y.-T., Chen, L.-M., Wong, K.-T., Huang, H.-M., Chen, C.-H., Chang, Y.J., Huang, C.-C., Liu, T.-M., 2022. A universal strategy for the fabrication of single-photon and multiphoton NIR nanoparticles by loading organic dyes into water-soluble polymer nanosponges. J Nanobiotechnol 20, 311. https://doi.org/10.1186/s12951-022-01515-5

Yang, Z., Zhao, Y., Hao, Y., Li, X., Zvyagin, A.V., Whittaker, A.K., Cui, Y., Yang, B., Lin, Q., Li, Y., 2021. Ultrasmall Red Fluorescent Gold Nanoclusters for Highly Biocompatible and Long-Time Nerve Imaging. Part. Part. Syst. Charact. 38, 2100001. https://doi.org/10.1002/ppsc.202100001

Yoshino, F., Amano, T., Zou, Y., Xu, J., Kimura, F., Furusho, Y., Chano, T., Murakami, T., Zhao, L., Komatsu, N., 2019. Preferential Tumor Accumulation of Polyglycerol Functionalized Nanodiamond Conjugated with Cyanine Dye Leading to Near-Infrared Fluorescence In Vivo Tumor Imaging. Small 15, 1901930. https://doi.org/10.1002/smll.201901930

Yu, C., Harbich, W., Sementa, L., Ghiringhelli, L., Aprá, E., Stener, M., Fortunelli, A., Brune, H., 2017. Intense fluorescence of Au_{20}. The Journal of Chemical Physics 147, 074301. https://doi.org/10.1063/1.4996687

Yu, S.-J., Kang, M.-W., Chang, H.-C., Chen, K.-M., Yu, Y.-C., 2005. Bright Fluorescent Nanodiamonds: No Photobleaching and Low Cytotoxicity. J. Am. Chem. Soc. 127, 17604–17605. https://doi.org/10.1021/ja0567081

Yu, Y., Luo, Z., Chevrier, D.M., Leong, D.T., Zhang, P., Jiang, D., Xie, J., 2014. Identification of a Highly Luminescent $Au_{22}(SG)_{18}$ Nanocluster. J. Am. Chem. Soc. 136, 1246–1249. https://doi.org/10.1021/ja411643u

Yuan, J., Müller, A.H.E., Matyjaszewski, K., Sheiko, S.S., 2012. Molecular Brushes, in: Polymer Science: A Comprehensive Reference. Elsevier, pp. 199–264. https://doi.org/10.1016/B978-0-444-53349-4.00164-3

Yuan, S.-F., Li, J.-J., Guan, Z.-J., Lei, Z., Wang, Q.-M., 2020. Ultrastable hydrido gold nanoclusters with the protection of phosphines. Chem. Commun. 56, 7037–7040. https://doi.org/10.1039/D0CC02339F

Yuan, X., Zhang, B., Luo, Z., Yao, Q., Leong, D.T., Yan, N., Xie, J., 2014. Balancing the Rate of Cluster Growth and Etching for Gram-Scale Synthesis of Thiolate-Protected Au_{25} Nanoclusters with Atomic Precision. Angew. Chem. Int. Ed. 53, 4623–4627. https://doi.org/10.1002/anie.201311177

Yue, D., Wang, M., Deng, F., Yin, W., Zhao, H., Zhao, X., Xu, Z., 2018. Biomarker-targeted fluorescent probes for breast cancer imaging. Chinese Chemical Letters 29, 648–656. https://doi.org/10.1016/j.cclet.2018.01.046

Zhang, P., Yang, X.X., Wang, Y., Zhao, N.W., Xiong, Z.H., Huang, C.Z., 2014. Rapid synthesis of highly luminescent and stable Au_{20} nanoclusters for active tumor-targeted imaging in vitro and in vivo. Nanoscale 6, 2261–2269. https://doi.org/10.1039/C3NR05269A

Zhang, T., Liu, G.-Q., Leong, W.-H., Liu, C.-F., Kwok, M.-H., Ngai, T., Liu, R.-B., Li, Q., 2018. Hybrid nanodiamond quantum sensors enabled by volume phase transitions of hydrogels. Nature Communications 9, 3188. https://doi.org/10.1038/s41467-018-05673-9

Zhang, X., Fu, C., Feng, L., Ji, Y., Tao, L., Huang, Q., Li, S., Wei, Y., 2012. PEGylation and polyPEGylation of nanodiamond. Polymer 53, 3178–3184. https://doi.org/10.1016/j.polymer.2012.05.029

Zhang, X.-D., Wu, D., Shen, X., Liu, P.-X., Fan, F.-Y., Fan, S.-J., 2012. In vivo renal clearance, biodistribution, toxicity of gold nanoclusters. Biomaterials 33, 4628–4638. https://doi.org/10.1016/j.biomaterials.2012.03.020

Zhang, Y., Guo, S., Wei, C., 2022. Fluorescence Spectroscopy: Part I Principles, in: Reference Module in Earth Systems and Environmental Sciences. Elsevier, p. B9780128229743002000. https://doi.org/10.1016/B978-0-12-822974-3.00081-1

Zhao, L., Nakae, Y., Qin, H., Ito, T., Kimura, T., Kojima, H., Chan, L., Komatsu, N., 2014a. Polyglycerol-functionalized nanodiamond as a platform for gene delivery: Derivatization, characterization, and hybridization with DNA. Beilstein Journal of Organic Chemistry 10, 707–713. https://doi.org/10.3762/bjoc.10.64

Zhao, L., Xu, Y.-H., Akasaka, T., Abe, S., Komatsu, N., Watari, F., Chen, X., 2014b. Polyglycerol-coated nanodiamond as a macrophage-evading platform for selective drug delivery in cancer cells. Biomaterials 35, 5393–5406. https://doi.org/10.1016/j.biomaterials.2014.03.041

Zheng, F., Huang, X., Ding, J., Bi, A., Wang, S., Chen, F., Zeng, W., 2022. NIR-I Dye-Based Probe: A New Window for Bimodal Tumor Theranostics. Front. Chem. 10, 859948. https://doi.org/10.3389/fchem.2022.859948

Zheng, J., Zhou, C., Yu, M., Liu, J., 2012. Different sized luminescent gold nanoparticles. Nanoscale 4, 4073–4083. https://doi.org/10.1039/C2NR31192E

Zheng, Q., Lavis, L.D., 2017. Development of photostable fluorophores for molecular imaging. Current Opinion in Chemical Biology 39, 32–38. https://doi.org/10.1016/j.cbpa.2017.04.017

Zheng, Y., Lai, L., Liu, W., Jiang, H., Wang, X., 2017. Recent advances in biomedical applications of fluorescent gold nanoclusters. Advances in Colloid and Interface Science 242, 1–16. https://doi.org/10.1016/j.cis.2017.02.005

Zhou, C., Hao, G., Thomas, P., Liu, J., Yu, M., Sun, S., Öz, O.K., Sun, X., Zheng, J., 2012. Near-Infrared Emitting Radioactive Gold Nanoparticles with Molecular Pharmacokinetics. Angew. Chem. Int. Ed. 51, 10118–10122. https://doi.org/10.1002/anie.201203031

Zhou, M., Zeng, C., Li, Q., Higaki, T., Jin, R., 2019. Gold Nanoclusters: Bridging Gold Complexes and Plasmonic Nanoparticles in Photophysical Properties. Nanomaterials 9, 933. https://doi.org/10.3390/nano9070933

Zhou, M., Zhong, J., Wang, S., Guo, Q., Zhu, M., Pei, Y., Xia, A., 2015. Ultrafast Relaxation Dynamics of Luminescent Rod-Shaped, Silver-Doped Ag_xAu_{25-x} Clusters. J. Phys. Chem. C 119, 18790–18797. https://doi.org/10.1021/acs.jpcc.5b05376

Zhou, Z., Zhang, C., Qian, Q., Ma, J., Huang, P., Zhang, X., Pan, L., Gao, G., Fu, H., Fu, S., Song, H., Zhi, X., Ni, J., Cui, D., 2013. Folic acid-conjugated silica capped gold nanoclusters for targeted fluorescence/X-ray computed tomography imaging. J Nanobiotechnol 11, 17. https://doi.org/10.1186/1477-3155-11-17

Zhu, M., Aikens, C.M., Hollander, F.J., Schatz, G.C., Jin, R., 2008. Correlating the Crystal Structure of A Thiol-Protected Au25 Cluster and Optical Properties. J. Am. Chem. Soc. 130, 5883–5885. https://doi.org/10.1021/ja801173r

Zhu, Y., 2012. The Biocompatibility of Nanodiamonds and Their Application in Drug Delivery Systems. Theranostics 2, 302–312. https://doi.org/10.7150/thno.3627

8 LIST OF APPENDICES

Appendix A

Kvakova, K.; Ondra, M.; Schimer, J.; Petrik, M.; Novy, Z.; Raabova, H.; Hajduch, M.; Cigler, P. Visualization of Sentinel Lymph Nodes with Mannosylated Fluorescent Nanodiamonds. *Adv Funct Materials* 2022.

Appendix B

Petrini, G.; Tomagra, G.; Bernardi, E.; Moreva, E.; Traina, P.; Marcantoni, A.; Picollo, F.; **Kvaková, K.**; Cígler, P.; Degiovanni, I. P.; Carabelli, V.; Genovese, M. Nanodiamond–Quantum Sensors Reveal Temperature Variation Associated to Hippocampal Neurons Firing. *Adv. Sci.* 2022.

Appendix C

Pramanik, G.; Keprova, A.; Valenta, J.; Bocan, V.; **Kvaková, K.**; Libusova, L.; Cigler, P. Synthesis of Near-Infrared Emitting Gold Nanoclusters for Biological Applications. *JoVE* 2020.

Appendix D

Pramanik, G.; **Kvakova, K.**; Thottappali, M. A.; Rais, D.; Pfleger, J.; Greben, M.; El-Zoka, A.; Bals, S.; Dracinsky, M.; Valenta, J.; Cigler, P. Inverse Heavy-Atom Effect in near Infrared Photoluminescent Gold Nanoclusters. *Nanoscale* 2021.

Appendix E

Valenta, J.; Greben, M.; Pramanik, G.; **Kvakova, K.**; Cigler, P. Reversible Photo- and Thermal-Effects on the Luminescence of Gold Nanoclusters: Implications for Nanothermometry. *Phys. Chem. Chem. Phys.* 2021.

Appendix F

Pavelka, O.; **Kvakova, K.**; Vesely, J.; Mizera, J.; Cigler, P.; Valenta, J. Optically Coupled Gold Nanostructures: Plasmon Enhanced Luminescence from Gold Nanorod-Nanocluster Hybrids. *Nanoscale* 2022.

Appendix G

Pavelka, O.; Dyakov, S. A.; **Kvakova, K**.; Vesely, J.; Cigler, P.; Valenta, J. Towards Site-Specific Emission Enhancement of Gold Nanoclusters Using Plasmonic Systems: Advantages and Limitations. *Nanoscale* 2023.